Effects of cardiomyopathy-linked mutations K15N and R21H in tropomyosin on thin-filament regulation and pointed-end dynamics

Thu Ly[a,*], Christopher T. Pappas[b], Dylan Johnson[c], William Schlecht[a,d], Mert Colpan[b], Vitold E. Galkin[e], Carol C. Gregorio[b], Wen-Ji Dong[a,d], and Alla S. Kostyukova[a,*]

[a]Voiland School of Chemical Engineering and Bioengineering and [d]Department of Integrative Physiology and Neuroscience, Washington State University, Pullman, WA 99164; [b]Department of Cellular and Molecular Medicine and Sarver Molecular Cardiovascular Research Program, University of Arizona, Tucson, AZ 85721; [c]Department of Biochemistry and Molecular Biology, Brody School of Medicine at East Carolina University, Greenville, NC 27834; [e]Department of Physiological Sciences, Eastern Virginia Medical School, Norfolk, VA 23507

ABSTRACT **Missense mutations K15N and R21H in striated muscle tropomyosin are linked to dilated cardiomyopathy (DCM) and hypertrophic cardiomyopathy (HCM), respectively. Tropomyosin, together with the troponin complex, regulates muscle contraction and, along with tropomodulin and leiomodin, controls the uniform thin-filament lengths crucial for normal sarcomere structure and function. We used Förster resonance energy transfer to study effects of the tropomyosin mutations on the structure and kinetics of the cardiac troponin core domain associated with the Ca^{2+}-dependent regulation of cardiac thin filaments. We found that the K15N mutation desensitizes thin filaments to Ca^{2+} and slows the kinetics of structural changes in troponin induced by Ca^{2+} dissociation from troponin, while the R21H mutation has almost no effect on these parameters. Expression of the K15N mutant in cardiomyocytes decreases leiomodin's thin-filament pointed-end assembly but does not affect tropomodulin's assembly at the pointed end. Our in vitro assays show that the R21H mutation causes a twofold decrease in tropomyosin's affinity for F-actin and affects leiomodin's function. We suggest that the K15N mutation causes DCM by altering Ca^{2+}-dependent thin-filament regulation and that one of the possible HCM-causing mechanisms by the R21H mutation is through alteration of leiomodin's function.**

Monitoring Editor
Laurent Blanchoin
CEA Grenoble

Received: Jul 5, 2018
Revised: Oct 30, 2018
Accepted: Nov 14, 2018

INTRODUCTION

Many missense mutations in Tpm1.1, the predominant tropomyosin (Tpm) isoform in striated muscle, are linked to dilated cardiomyopathy (DCM) and hypertrophic cardiomyopathy (HCM) (Redwood and Robinson, 2013). DCM is characterized by ventricular chamber dilation and systolic dysfunction (Hershberger and Morales, 1993) and is the most common form of cardiomyopathy that leads to heart transplants in children and adults (Maron *et al.*, 2006; Sweet *et al.*, 2015; Rusconi *et al.*, 2017). HCM is the leading cause of sudden cardiac death in young people (Maron *et al.*, 2009; Frey *et al.*, 2011) and is defined by thickening of the ventricular walls with significant cellular disarray and myocardial scarring (Maron, 2002). Two Tpm1.1 mutations, K15N and R21H, are identified in patients diagnosed with DCM and HCM, respectively (Hershberger *et al.*, 2010; Fokstuen *et al.*, 2011). Both mutations have been shown to alter the structure of Tpm1.1 near the N-terminus (Colpan *et al.*, 2016b; Ly *et al.*, 2018). The K15N mutation reduces tropomyosin's affinity for F-actin, tropomodulin (Tmod), and leiomodin (Lmod) (Colpan *et al.*, 2016b, 2017). Another important binding partner of Tpm1.1 in cardiac tissue is the cardiac troponin complex (cTn). As such, we sought to

This article was published online ahead of print in MBoC in Press (http://www.molbiolcell.org/cgi/doi/10.1091/mbc.E18-06-0406) on November 21, 2018.

*Address correspondence to: Alla S. Kostyukova (alla.kostyukova@wsu.edu); Thu Ly (thu.ly@wsu.edu).

Abbreviations used: cTn, cardiac troponin; cTnI-I, inhibitory region of cardiac troponin I; cTnI-M, mobile domain of cardiac troponin I; cTnI-R, regulatory region of cardiac troponin I; DCM, dilated cardiomyopathy; FRET, Förster resonance energy transfer; FWHM, full width at half maximum; HCM, hypertrophic cardiomyopathy; Lmod2, leiomodin 2; N-cTnC, N-terminal domain of cardiac troponin C; TCSPC, time-correlated single photon counting; TEM, transmission electron microscopy; Tmod1, tropomodulin 1; Tpm1.1, striated muscle tropomyosin.

obtain a clearer picture of how these mutations lead to disease by investigating their impact on Tpm1.1's interaction with not only actin, Tmod, and Lmod but also cTn.

In cardiac muscle, actin-based thin filaments and myosin-based thick filaments form repeating contractile units called sarcomeres. Tpm1.1 stabilizes thin filaments by forming continuous polymers along the filament through head-to-tail association. Tpm1.1 is crucial for cardiac muscle contraction (for reviews, see Geeves, 2012, and Gunning *et al.*, 2015) where it interacts with cTn and regulates the interaction between actin and myosin. Muscle contraction is regulated both by intracellular Ca^{2+} levels and by the binding of myosin to actin, depicted by a model where thin filaments exist in equilibrium between three states (McKillop and Geeves, 1993; Pirani *et al.*, 2005; Poole *et al.*, 2006; Risi *et al.*, 2017). cTn consists of three subunits: troponin C (cTnC), troponin I (cTnI), and troponin T (cTnT). In the absence of Ca^{2+}, the hydrophobic pocket within the N-terminal domain of cTnC (N-cTnC) is closed, and both the inhibitory region (cTnI-I, residues 130–149) and mobile domain (cTnI-M, residues 167–211) of cTnI bind strongly to actin. Ca^{2+} binding to the single regulatory site within N-cTnC increases the opening of the hydrophobic pocket within this domain, allowing N-cTnC to associate with the regulatory region of cTnI (cTnI-R, residues 150–165) and subsequently interact with cTnI-I and cTnI-M. These structural changes propagate through cTnT to Tpm1.1, causing Tpm1.1's position on F-actin to change, exposing myosin-binding sites on actin's surface, thereby enabling actomyosin interactions underlying muscle contraction.

Thin filaments are polar with pointed ends, oriented toward the M-line, and barbed ends, attached to the Z-lines. Not only does Tpm1.1 stabilize and protect the thin filament from severing proteins, it also recruits Tmod and Lmod, Tmod's homologue, to the pointed end (Gregorio and Fowler, 1995; Tsukada *et al.*, 2010; Ly *et al.*, 2016) where they play crucial roles in regulating thin-filament assembly dynamics. Tmod1 and Lmod2 are the major isoforms found in cardiac tissues (Conley *et al.*, 2001). Tmod1 is an efficient pointed-end capping protein (Weber *et al.*, 1994, 1999), while Lmod2 does not completely prevent the filament to grow from the pointed end (Tsukada *et al.*, 2010; Pappas *et al.*, 2015). It is clear that both Tmod1 and Lmod2 are required for normal heart development. Loss of Tmod1 resulted in failure of early myofibril formation and embryonic lethality (Fritz-Six *et al.*, 2003), and knockout of Lmod2 led to shorter thin filaments, dilated cardiomyopathy, and lethality in juvenile mice (Pappas *et al.*, 2015). According to a model suggested by Tsukada and coauthors, Tmod1 and Lmod2 work together in the presence of Tpm1.1 to maintain the uniform lengths of thin filaments that are critical for normal sarcomere architecture and function (Tsukada *et al.*, 2010).

The K15N and R21H mutations are found within the first actin-binding site of Tpm1.1 and are located in the position *a* and *g* of the coiled-coil heptad repeat, respectively (Parry and Squire, 1973; McLachlan and Stewart, 1976; Singh and Hitchcock-DeGregori, 2007; Li *et al.*, 2011). The mutations are located several amino acid residues apart from each other, but they are linked to different types of cardiomyopathies that cause opposite phenotypic responses of the heart. In general, in vitro functional assays demonstrate that DCM-causing mutations in thin-filament regulatory proteins decrease Ca^{2+} sensitivity of contractile function, whereas HCM-causing mutations tend to increase it (Hernandez *et al.*, 2001; Robinson *et al.*, 2002; Mirza *et al.*, 2005, 2007).

To investigate whether the K15N and R21H mutations impose opposite effects on Ca^{2+}-dependent cardiac thin-filament regulation, we monitored structural and kinetic changes in cTn when thin filaments were under a free-Ca^{2+} or high-Ca^{2+} condition by means of Förster resonance energy transfer (FRET). We labeled residues 151 or 167 of cTnI with 5-((((2-iodoacetyle)amino)ethyl)amino)naphthalene-1-sulfonic acid (IAEDANS) as FRET donors and residue 89 of cTnC with N-(4-dimethylamino-3,5-dinitrophenyl)maleimide (DDPM) as a FRET acceptor. We found that the K15N mutation in Tpm1.1 increases donor–acceptor separation distances, reduces Ca^{2+} sensitivity of reconstituted cardiac thin filaments, and decreases the rate of cTnI-R's dissociation from N-cTnC triggered by the removal of Ca^{2+} from N-cTnC, while the R21H mutation has almost no effect on these parameters. Our in vitro assays show that the R21H mutation causes a twofold decrease in Tpm's affinity for F-actin and affects Lmod2's function. Visualization of filament bundling by Lmod2 using transmission electron microscopy (TEM) suggest that the R21H mutation in Tpm1.1 may alter the way Lmod2 associates with the sides of F-actin. Expression of the K15N mutant in rat cardiomyocytes decreases Lmod2's thin-filament pointed-end assembly but does not affect Tmod1's assembly at the pointed end. We suggest that the K15N mutation cause DCM mainly by altering Ca^{2+}-dependent thin-filament regulation. Data obtained for the R21H mutation shed light on possible mechanisms underlying development of HCM, one of which involves the alteration of Lmod2's function.

RESULTS

Effects of the K15N and R21H mutations in Tpm1.1 on Ca^{2+}-dependent cardiac thin-filament regulation

The R21H mutation in Tpm1.1 decreases Tpm's affinity for F-actin by twofold. The major function of Tpm1.1 revolves around regulating muscle contraction, which is strongly dependent on Tpm1.1's binding affinity for F-actin. One of the first steps in understanding the molecular consequences of a mutation in Tpm1.1 is to determine how the mutation affects its affinity for actin. We have previously determined that the K15N mutation leads to a threefold decrease in the affinity of Tpm1.1 for F-actin (Colpan *et al.*, 2017).

Since residue Arg-21 is located next to residue Asp-20 in Tpm1.1, which is suggested to make direct contact with residues Arg-147, Lys-326, and Lys-328 in actin (Li *et al.*, 2011), we speculated that the R21H mutation may alter Tpm1.1's binding affinity for F-actin. To test this hypothesis, we conducted experiments where wild-type (WT) or mutated Tpm1.1 cosediments with F-actin (Figure 1). The amounts of actin and Tpm1.1 in the pellets, as well as those of Tpm1.1 in the supernatants, were quantified. The data were fitted to both the Hill model and the McGhee and von Hippel model, from which values of K_{app} and K_o, respectively, were obtained. These binding constants representing Tpm1.1's affinity for F-actin are summarized in Table 1. Tpm1.1[R21H] displays a ~twofold decrease in affinity for F-actin when compared with WT Tpm1.1.

Tpm1.1[K15N] decreases Ca^{2+} sensitivity of reconstituted cardiac thin filaments. In general, DCM-causing mutations in thin-filament regulatory proteins decrease Ca^{2+} sensitivity of contractile function, whereas HCM-causing mutations tend to increase it (Hernandez *et al.*, 2001; Robinson *et al.*, 2002; Mirza *et al.*, 2005, 2007). Intrigued by the question of whether the K15N and R21H mutations have opposite effects on Ca^{2+}-dependent cardiac thin-filament regulation, we conducted FRET measurements monitoring structural changes within the regulatory head of the cTn core domain, consisting of N-cTnC and cTnI-R, in the presence of Tpm1.1 (WT or mutated). The probes for these measurements are IAEDANS, which is attached to either residue 151 or residue 167 in cTnI, and DDPM, which is attached to residue 89 in cTnC. These probes form two

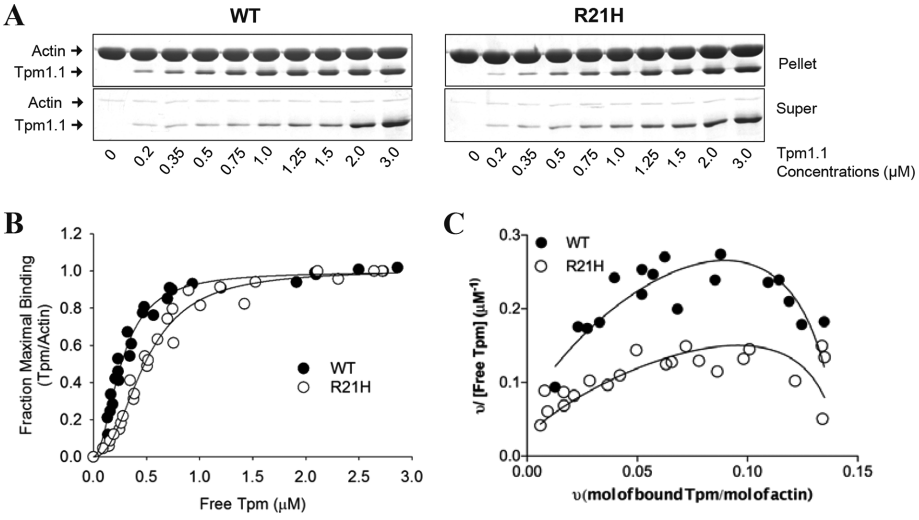

FIGURE 1: The R21H mutation causes a twofold decrease in Tpm1.1's affinity for F-actin. Binding of Tpm1.1 (WT or R21H) to F-actin was measured by cosedimentation. (A) Tpm1.1 (0–3 μM) was combined with 5 μM F-actin and cosedimented at 20°C in 2 mM Tris–HCl, pH 8.0, 25 mM imidazole, 100 mM KCl, 2 mM $MgCl_2$, 1 mM EGTA, 0.2 mM $CaCl_2$, 0.01% NaN_3, 0.5 mM DTT, and 0.2 mM ATP. Pellets and supernatants were run on 10% polyacrylamide SDS gels and stained with Coomassie-blue. (B) Fraction maximal binding representing the stoichiometric binding of one Tpm1.1 per seven actin molecules was obtained from band density ratios of Tpm and actin in the pellet samples. Free-Tpm concentration in the supernatants was determined using a standard curve established at known Tpm concentrations. The data ($n = 3$) were fitted to the Hill equation to estimate the apparent binding constant (K_{app}). (C) Analysis of Tpm's affinity for F-actin using the McGhee–von Hippel model to estimate the association constant (K_o). The binding constants obtained from fitting the data to both models are reported in Table 1.

separate FRET pairs, cTnI[S151$C_{IAEDANS}$] – cTnC[S89C_{DDPM}] and cTnI[S167$C_{IAEDANS}$] – cTnC[S89C_{DDPM}]. Using these probes, the interaction between N-cTnC and cTnI-R was monitored to determine effects of the Tpm1.1 mutations on Ca^{2+}-dependent thin-filament regulation.

In steady-state Ca^{2+} titration experiments, FRET permits the tracking of changes in cTnI-cTnC separation due to the addition of Ca^{2+}. Binding of Ca^{2+} to N-cTnC leads to the association of cTnI-R with a hydrophobic patch within Ca^{2+}-saturated N-cTnC, thereby removing cTnI-I from actin and enabling cTnI-I to interact with cTnC. Since residue 151 and residue 167 are located near the N-terminus and C-terminus of cTnI-R, respectively, their individual distances to residue 89, which is located within the central linker region of cTnC (close to N-TnC), are shortened as a result of these Ca^{2+}-induced structural changes. As Ca^{2+} concentration increases, the monitored donor (IAEDANS) emission intensity decreases due to an increase in FRET efficiency.

	Hill model	McGhee and von Hippel model
	K_{app} (μM^{-1})	K_o (μM^{-1})
WT	3.82 ± 0.30	0.061 ± 0.010
R21H	2.01 ± 0.22**	0.023 ± 0.021*

Each value is reported as mean ± SD. Asterisks indicate statistically significant differences from WT using one-way analysis of variance (ANOVA) with Holm-Sidak post-hoc test (*$p < 0.05$ and **$p < 0.01$).

TABLE 1: Binding constants determined from Tpm1.1's cosedimentation with F-actin by fitting the data ($n = 3$) to the Hill equation and the McGhee–von Hippel equation.

Figure 2 demonstrates representative titration data in which the normalized FRET efficiency is plotted against pCa. Titration data were fitted to the Hill equation to obtain pCa_{50} values (Table 2). A pCa_{50} value is an indicator of the thin filament's Ca^{2+} sensitivity. Thin filaments carrying the cTnI[S151$C_{IAEDANS}$]–cTnC[S89C_{DDPM}] FRET pair have higher pCa_{50} values than those carrying the cTnI[S167$C_{IAEDANS}$] – cTnC[S89C_{DDPM}] FRET pair (Table 2), which is consistent with those reported in Schlecht *et al.* (2014). Under physiological conditions, muscle contraction is regulated by both Ca^{2+} and cross-bridge formation. Myosin S1 was added to the thin-filament complex prior to the titration. In the presence of myosin S1, pCa_{50} values increase (Table 2) due to an increase in N-cTnC's affinity for Ca^{2+} as previously observed (Xing *et al.*, 2009; Schlecht *et al.*, 2014). It is well known that myosin crossbridges increase the affinity of cTnC for Ca^{2+} (Guth and Potter, 1987; Wang *et al.*, 1999).

Values of pCa_{50} are used to compare Ca^{2+} sensitivities between thin-filament samples containing WT Tpm1.1, Tpm1.1[K15N], or Tpm1.1[R21H]. Regardless of whether myosin S1 is present, Tpm1.1[K15N] appears to desensitize the thin filament to Ca^{2+}. Tpm1.1[R21H] affects only the myosin S1-bound thin filaments carrying the cTnI[S167$C_{IAEDANS}$]–cTnC[S89C_{DDPM}] FRET pair: they are more sensitive to Ca^{2+} in the presence of Tpm1.1[R21H] than in the presence of WT Tpm1.1 (Table 2).

Tpm1.1[K15N] increases the distance between cTnI-R and N-cTnC. To understand how the changes in Ca^{2+} sensitivity caused by Tpm1.1[K15N] correlate with structural changes within the cTn core domain, specifically changes in the distance between cTnI-R and N-cTnC, time-correlated single photon counting (TCSPC) fluorescence intensity decays of the donor were measured in the absence or presence of the acceptor. Figure 3A shows representative TCSPC fluorescence decays of the donor cTnI[S167$C_{IAEDANS}$] in the presence of the acceptor cTnC[S89C_{DDPM}]. By measuring the reduction in the characteristic decay time of the donor, which occurs as a function of the acceptor proximity, the interprobe distance distribution was determined. Each interprobe distance distribution is represented by a Gaussian (Figure 3B), with characteristic parameters of mean interprobe distance ($\overline{r}$) and full width at half maximum (FWHM) of the distribution. The mean interprobe distance when thin filaments were under a free-Ca^{2+} condition and that when thin filaments were under a high, saturating Ca^{2+} condition were determined. These parameters are summarized in Table 3. FWHM is directly related to the mobility of the donor relative to the acceptor and therefore provides a metric of interprobe flexibility (Robinson *et al.*, 2004). A small FWHM value indicates a lack of interprobe mobility and structural flexibility, which occurs when cTnI-R binds to the hydrophobic pocket of Ca^{2+}-bound N-cTnC. The switching distance, denoted as r_{sw} hereafter, which is the difference in the mean interprobe distance between the free- and high-Ca^{2+} conditions, is calculated for each thin-filament sample and displayed in Figure 3C.

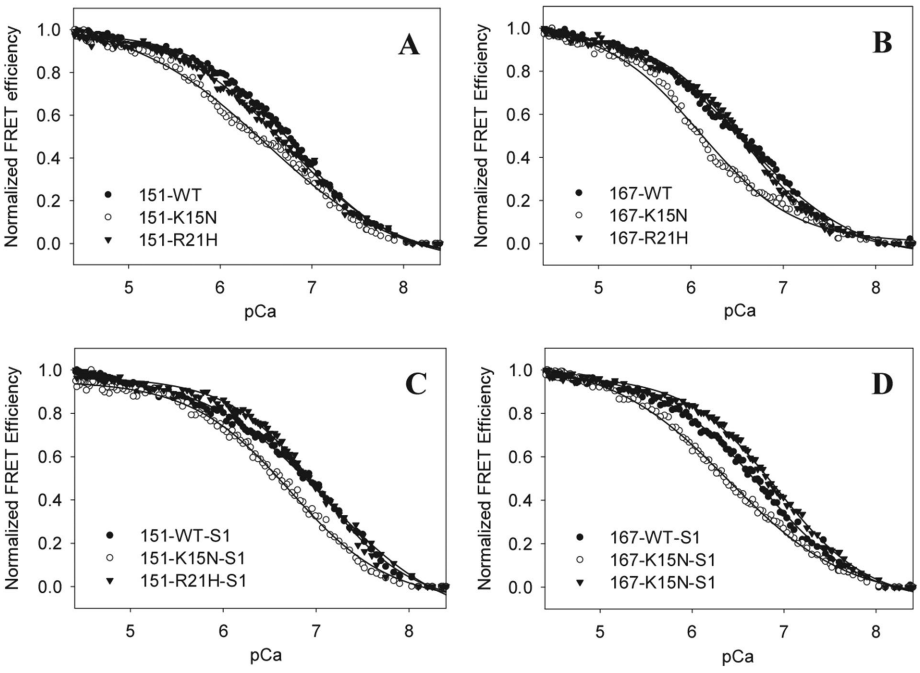

FIGURE 2: The K15N mutation in Tpm1.1 decreases Ca^{2+} sensitivity of reconstituted cardiac thin filaments. Steady-state Ca^{2+} titrations of thin filaments carrying cTnI[S151$C_{IAEDANS}$ or S167$C_{IAEDANS}$] and cTnC[S89C_{DDPM}] in the absence (A, B) or presence (C, D) of myosin S1. Thin filaments were reconstituted in the presence of WT or mutated (K15N or R21H) Tpm1.1.

As reported in Table 3, the interprobe distances decrease on Ca^{2+} saturation, each of which is accompanied by a decrease in FWHM. In the presence of WT Tpm1.1, Ca^{2+} saturation results in an approximate 6.2-Å and 8.1-Å reduction in interprobe distance in thin filaments containing cTnI[S151$C_{IAEDANS}$] and cTnI[S167$C_{IAEDANS}$], respectively. This reduction in the interprobe distance is expected because cTnI-R comes in contact with N-cTnC on Ca^{2+} saturation. The decrease in FWHM value on Ca^{2+} saturation, again indicating reduced interprobe flexibility, was previously observed (Ouyang *et al.*, 2010; Zhou *et al.*, 2012). Values of FWHM slightly decrease when myosin S1 is present, analogously to previous observations (Ouyang *et al.*, 2010; Schlecht *et al.*, 2014).

While Tpm1.1[R21H] does not produce any effect on the interprobe distance under different biochemical conditions, thin filaments carrying Tpm1.1[K15N] show noticeably greater mean interprobe distances than those seen in WT Tpm1.1-containing filaments (Table 3). This effect of Tpm1.1[K15N] on the interprobe distance is not altered on addition of myosin S1. As Tpm1.1[K15N] increases the mean interprobe distance to a similar extent when filaments are under a free-Ca^{2+} condition or when they are under a high-Ca^{2+} condition, r_{sw} is essentially the same as that observed in WT Tpm1.1-containing thin filaments (Figure 3C).

cTnI$_{IAEDANS}$ – Tpm1.1 (n = 7–10)	Thin filament	Thin filament + myosin S1
S151C – WT	6.79 ± 0.01	7.05 ± 0.01
S151C – K15N	6.68 ± 0.03***	6.92 ± 0.02**
S151C – R21H	6.77 ± 0.03	7.03 ± 0.03
S167C – WT	6.54 ± 0.01	6.77 ± 0.01
S167C – K15N	6.28 ± 0.06***	6.57 ± 0.04***
S167C – R21H	6.56 ± 0.02	6.83 ± 0.03*

Each value is reported as mean ± SD. Asterisks indicate statistically significant differences from WT using one-way ANOVA with Holm-Sidak post-hoc test (*p < 0.05, **p < 0.01, and ***p < 0.001).

TABLE 2: Parameter pCa_{50} obtained from steady-state Ca^{2+} titration measurements.

Tpm1.1[K15N] decreases the rate of cTnI-R's dissociation from N-cTnC following the removal of Ca^{2+} from N-cTnC. We next examined the effect of both mutations in Tpm1.1 on the deactivation kinetics of thin filaments. Conformational changes in the core domain of cTn induced by the dissociation of Ca^{2+} from N-cTnC were monitored as a function of time using FRET stopped-flow measurements. In these measurements, thin filaments were first saturated with Ca^{2+}. 1,2-bis(2-aminophenoxy)ethane-*N*,*N*,*N*′,*N*′-tetraacetic acid (BAPTA), a strong Ca^{2+}-specific chelator, was used to quickly remove Ca^{2+} from N-cTnC. FRET is used to measure the progress of the conformational transition as reconstituted cardiac thin filaments switch from being under a high-Ca^{2+} condition to being under a free-Ca^{2+} condition. As one would expect, the emission intensity of the donor increases due to a decrease in FRET efficiency as cTnI-R moves away from N-cTnC. Figure 4 represents typical stopped-flow kinetic traces, where the rapid increase in the donor fluorescence is monitored. Rate constants associated with the dissociation of cTnI-R from N-cTnC due to the removal of Ca^{2+} from N-cTnC, referred to as I_R-C_N dissociation hereafter, are reported in Table 4.

I_R-C_N dissociation rates of WT Tpm1.1-containing thin filaments are ~34.0 s^{-1} and 43.7 s^{-1} for filaments with cTnI[S151$C_{IAEDANS}$] and cTnI[S167$C_{IAEDANS}$], respectively (Table 4). Faster I_R-C_N dissociation associated with the donor located closer to cTnI-M, cTnI[S167$C_{IAEDANS}$], was previously observed (Zhou *et al.*, 2012). Addition of myosin S1 reduces the thin-filament deactivation kinetics to different extents, which is also in agreement with previous studies (Zhou *et al.*, 2012; Schlecht *et al.*, 2014).

Thin filaments carrying Tpm1.1[K15N] show a decrease in the I_R-C_N dissociation rate, regardless of whether myosin S1 is present (Table 4). Tpm1.1[R21H]-containing thin filaments show no statistically significant change in I_R-C_N dissociation rate compared with WT Tpm1.1-containing thin filaments. Combining these results with those from the Ca^{2+} titration experiments, Tpm1.1[K15N] appears to reduce not only the sensitivity of thin filaments to Ca^{2+} but also their I_R-C_N dissociation kinetics, whereas Tpm1.1[R21H] has no effect on Ca^{2+}-binding behavior or on I_R-C_N dissociation kinetics of thin filaments.

Tpm1.1[K15N] decreases the rate of ATP hydrolysis by myosin S1 when thin filaments are at saturating Ca^{2+} concentrations. Mutations in Tpm1.1 can alter the ability of actin to stimulate the ATPase activity of myosin (Mathur *et al.*, 2011). In the presence of cTn, either the extent of inhibition at low Ca^{2+} levels or the extent of activation at saturating Ca^{2+} may be affected.

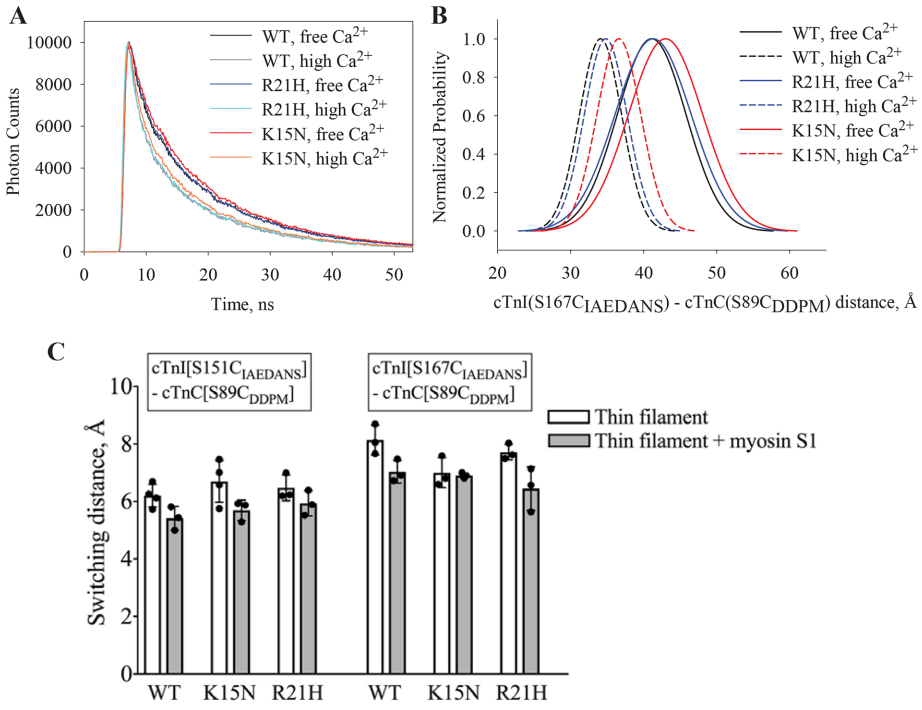

FIGURE 3: The K15N mutation in Tpm1.1 increases the interprobe distances in reconstituted cardiac thin filaments. (A) Time-resolved fluorescence decay curves for thin filaments carrying cTnI[S167$C_{IAEDANS}$] – cTnC[S89C_{DDPM}] in the presence of myosin S1. Thin filaments were reconstituted with WT or mutated (K15N or R21H) Tpm1.1. Measurements were carried out when thin filaments were under a free-Ca^{2+} condition or under a high-Ca^{2+} condition. (B) Distance distributions were derived from fitting of the fluorescence decay curves in A using DecayFit. (C) Switching distances calculated from values displayed in Table 2. Averages and standard deviations are shown by columns and error bars (n = 3–4), respectively.

The ATPase rate of myosin S1 was measured in the presence of actin regulated by cTn and WT Tpm1.1, Tpm1.1[K15N], or Tpm1.1[R21H]. Wild-type Tpm1.1 and both mutants display excellent regulation with more than a 25-fold difference in rate between very low and saturating Ca^{2+} (Supplemental Figure S1). At very low Ca^{2+} concentrations, there is not a statistically significant difference in ATPase rate determined for filaments containing WT and mutated Tpm1.1. At saturating Ca^{2+} concentrations, the ATPase rate measured for filaments containing Tpm1.1[K15N] is lower than that for WT Tpm1.1-containing filaments. There is a small increase in the ATPase rate measured in the presence of Tpm1.1[R21H]. However, this difference does not reach a statistical significance relative to WT Tpm1.1.

Effects of the R21H mutation in Tpm1.1 on Tmod1 and Lmod2's pointed-end capping abilities

Both Tmod1 and Lmod2 require Tpm1.1 to localize at the pointed end of the thin filament and their functions at the pointed end strongly depend on their binding to Tpm1.1 (Weber *et al.*, 1994; Gregorio and Fowler, 1995; Chereau *et al.*, 2008; Tsukada *et al.*, 2010; Ly *et al.*, 2016). We have previously demonstrated that the K15N mutation affects the pointed-end capping functions of both Tmod1 and Lmod2 (Colpan *et al.*, 2017). Here we examined effects of the R21H mutation in Tpm1.1 on Tmod1 and Lmod2's capping activities.

We have recently demonstrated that the R21H mutation causes a ~30-fold decrease in the binding affinity of αTM1a$_{1\text{-}28}$Zip, a chimeric peptide containing 28 N-terminal residues of Tpm1.1 to Lmod2s1, an Lmod2 fragment consisting of residues 2-41 (Ly *et al.*, 2018). On the basis of this result, we speculated that the R21H mutation may exert a

	Free Ca^{2+}		High Ca^{2+}	
cTnI – Tpm1.1 (n = 3–4)	$\bar{r}$ (Å)	FWHM (Å)	$\bar{r}$ (Å)	FWHM (Å)
		Thin filament		
S151$C_{IAEDANS}$ – WT	41.1 ± 1.0	12.1 ± 1.2	34.9 ± 0.9	6.8 ± 0.6
S151$C_{IAEDANS}$ – K15N	43.1 ± 2.3*	13.7 ± 2.1	36.4 ± 2.1*	7.2 ± 1.5
S151$C_{IAEDANS}$ – R21H	41.0 ± 1.3	13.0 ± 0.9	34.5 ± 1.7	7.3 ± 2.6
S167$C_{IAEDANS}$ – WT	42.4 ± 1.7	14.2 ± 2.5	34.3 ± 1.1	7.0 ± 1.7
S167$C_{IAEDANS}$ – K15N	43.6 ± 2.0	14.3 ± 1.5	36.6 ± 2.1*	6.5 ± 0.9
S167$C_{IAEDANS}$ – R21H	41.2 ± 1.8	14.7 ± 2.9	33.5 ± 2.3	6.8 ± 2.0
		Thin filament + myosin S1		
S151$C_{IAEDANS}$ – WT	39.5 ± 1.7	10.5 ± 1.0	34.0 ± 2.5	6.2 ± 0.7
S151$C_{IAEDANS}$ – K15N	41.4 ± 1.0*	11.4 ± 0.7	35.8 ± 1.0	6.9 ± 1.3
S151$C_{IAEDANS}$ – R21H	40.2 ± 2.0	10.9 ± 2.0	34.3 ± 1.1	6.0 ± 2.4
S167$C_{IAEDANS}$ – WT	41.1 ± 1.5	11.1 ± 1.7	34.1 ± 0.7	6.8 ± 0.9
S167$C_{IAEDANS}$ – K15N	42.5 ± 1.3	12.0 ± 2.0	35.6 ± 1.5*	7.1 ± 1.2
S167$C_{IAEDANS}$ – R21H	41.3 ± 1.7	12.3 ± 1.9	34.8 ± 2.0	6.9 ± 1.2

Each value is reported as mean ± SD. Asterisks indicate statistically significant differences from WT using one-way ANOVA with Holm-Sidak post-hoc test (*p < 0.05).

TABLE 3: Interprobe distance distribution parameters.

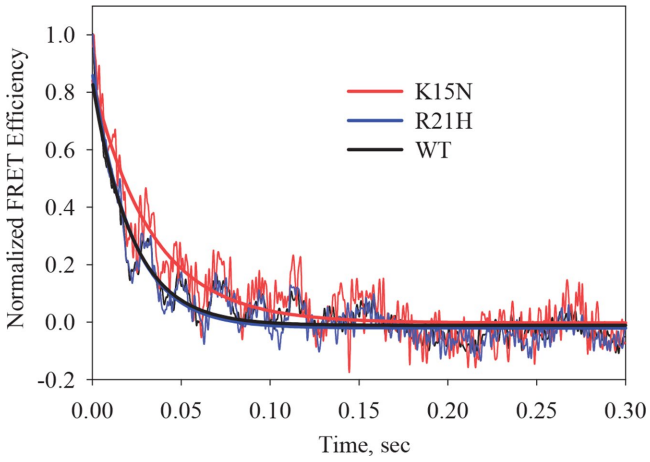

FIGURE 4: The K15N mutation in Tpm1.1 reduces the deactivation kinetics of reconstituted cardiac thin filaments induced by dissociation of Ca^{2+} from N-cTnC. Stopped-flow kinetic measurements for thin filaments labeled with cTnI[S167$C_{IAEDANS}$] – cTnC[S89C_{DDPM}] in the presence of myosin S1. Thin filaments were reconstituted with WT or mutated (K15N or R21H) Tpm1.1. Raw data were fitted to an exponential decay function using a built-in program associated with the KinTek instrument.

similar effect on the Tpm-dependent pointed-end capping ability of Lmod2. We questioned whether the mutation would change the ability of truncated Lmod2, $Lmod2_{1\text{-}514}$, to inhibit actin polymerization at the pointed end. $Lmod2_{1\text{-}514}$ lacks the WH2 domain, which is the third actin-binding site in Lmod2, and caps Tpm1.1-saturated F-actin in a similar manner to Tmod1 (Tsukada *et al.*, 2010). We performed a pyrene-actin polymerization assay to measure the rate of actin polymerization at the pointed end at saturating concentrations of Tpm1.1 (WT or mutated) in the presence of $Lmod2_{1\text{-}514}$ (Figure 5). While the rates of pointed-end polymerization in the presence of WT Tpm1.1 and Tpm1.1[R21H] are similar (Figure 5A), addition of $Lmod2_{1\text{-}514}$ noticeably decreases the actin polymerization kinetics but to a greater extent for WT Tpm1.1-saturated filaments than for Tpm1.1[R21H]-saturated filaments (Figure 5, B–D). $Lmod2_{1\text{-}514}$'s inhibition of pointed-end polymerization is much less effective in the presence of Tpm1.1[R21H] than in the presence of WT Tpm1.1.

We have previously determined that the R21H mutation in Tpm1.1 weakens the stability of complexes formed by $\alpha TM1a_{1\text{-}28}Zip$ and a Tmod1 peptide containing a Tpm-binding site, Tmod1s1 or Tmod1s2 (Ly *et al.*, 2018). However, the effect of the R21H mutation on $\alpha TM1a_{1\text{-}28}Zip$'s affinity for Tmod1s1 or Tmod1s2 could not be determined due to inability to calculate dissociation constants. We performed a pyrene-actin polymerization assay to test whether Tmod1's pointed-end capping ability was affected in the presence of Tpm1.1[R21H]. We saw that Tpm1.1[R21H] does not alter inhibition of pointed-end polymerization by Tmod1 (Supplemental Figure S2).

cTnI – Tpm1.1 (n = 3–4)	Thin filament	Thin filament + myosin S1
S151$C_{IAEDANS}$ – WT	31.0 ± 2.1	28.5 ± 3.4
S151$C_{IAEDANS}$ – K15N	29.2 ± 2.9	26.4 ± 1.2
S151$C_{IAEDANS}$ – R21H	30.6 ± 2.7	31.8 ± 1.8
S167$C_{IAEDANS}$ – WT	43.7 ± 1.1	34.9 ± 1.0
S167$C_{IAEDANS}$ – K15N	37.4 ± 1.2***	27.8 ± 0.7**
S167$C_{IAEDANS}$ – R21H	43.9 ± 2.3	35.2 ± 2.1

Each value is reported as mean ± SD. Asterisks indicate statistically significant differences from WT using one-way ANOVA with Holm-Sidak post-hoc test (**$p < 0.01$ and ***$p < 0.001$).

TABLE 4: I_R-C_N dissociation rates (s^{-1}) induced by Ca^{2+} dissociation from cTnC.

Effects of the K15N and R21H mutations on Tmod1 and Lmod2's thin-filament pointed-end assembly in rat neonatal cardiomyocytes

To test whether the K15N or R21H mutations affect Tmod1 and Lmod2's pointed-end assembly in cardiac muscle cells, we expressed mCherry-tagged versions of the mutations in rat neonatal cardiomyocytes via adenovirus. Immunoblot analysis revealed that the expression level of each construct was similar and approximately three times more than endogenous Tpm (Supplemental Figure S3). Sarcomeric assembly of the Tpm1.1 mutants is not noticeably different from that of WT Tpm1.1 in cardiomyocytes (Figure 6A). Immunofluorescence staining revealed a significant decrease in the number of cells with thin-filament pointed-end assembly of Lmod2 following expression of Tpm1.1[K15N] compared with WT Tpm1.1 (Figure 6). Expression of Tpm1.1[R21H] did not significantly change the assembly of Lmod2 (Figure 6). Lmod2 expression levels are unchanged in cells expressing Tpm1.1 mutants (Supplemental Figure S4). We also did not detect a change in the pointed-end assembly of Tmod1 on expression of either mutant (Supplemental Figure S5).

Effects of the K15N and R21H mutations on Lmod2's binding to the sides of F-actin

It has been shown that in sarcomeres Lmod2 displays distribution along the length of thin filaments (Skwarek-Maruszewska *et al.*, 2010; Tsukada *et al.*, 2010). In vitro cosedimentation assays indicate that Lmod2 may interact with the sides of F-actin (Skwarek-Maruszewska *et al.*, 2010; Szatmari *et al.*, 2017).

In this study, we used TEM to visualize complexes of F-actin and Lmod2 in the presence or absence of WT Tpm1.1 (Figure 7). F-actin forms bundles in the presence of Lmod2, suggesting that Lmod2 binds along the side of the filament. We presume that Lmod2, on binding to the side of a filament, interacts with adjacent actin filaments through at least one other actin-binding site. In the absence (Figure 7B) or presence (Figure 7C) of Tpm1.1, Lmod2 packs actin filaments into sparse thin bundles where individual actin filaments run in parallel (Figure 7, B and C, inserts).

To confirm our observations of the TEM images, we used centrifugation to separate individual actin filaments from F-actin bundles seen in the TEM samples, presuming that bundles may sediment at low centrifugation speeds while individual filaments should sediment at higher speeds. After Lmod2 was added to F-actin in the absence or presence of Tpm1.1, the samples were centrifuged at 4000 × *g*. At this speed, we expected bundles to be spun down while individual filaments should remain in the supernatant. The supernatants were then centrifuged at 213,600 × *g*. The pellets formed at each centrifugation step were analyzed using SDS–PAGE. The total pelleted actin combined from both steps was similar across all samples. At 4000 × *g*, the amounts of pelleted actin in the presence of Lmod2 were higher than those in the absence of Lmod2 (Figure 8), hence it is clear that addition of Lmod2 leads to formation of F-actin bundles. There is a slight but not statistically significant decrease in the amount of pelleted actin when Tpm1.1 is present.

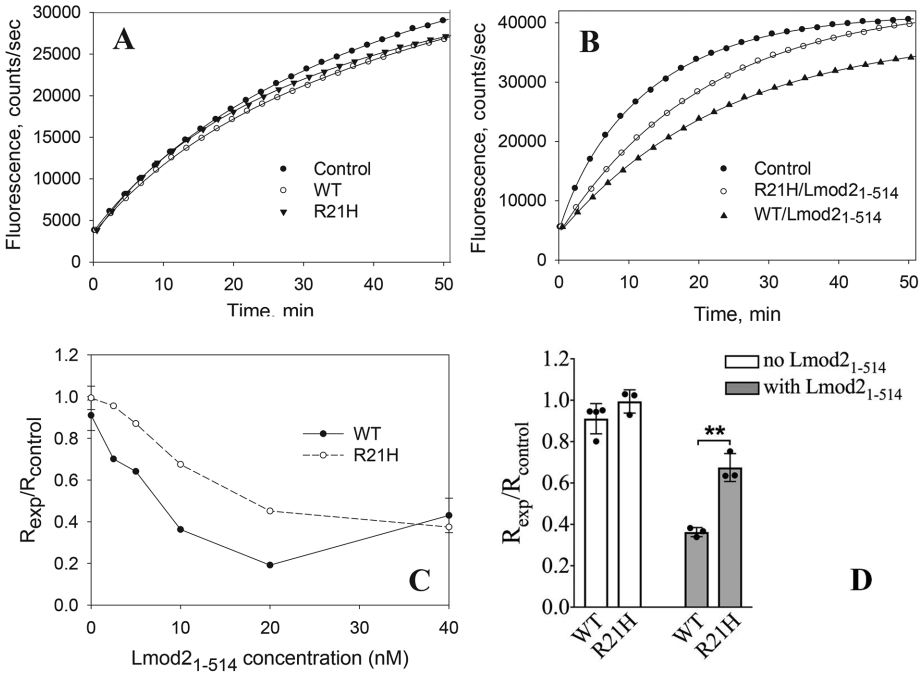

FIGURE 5: The R21H mutation in Tpm1.1 decreases pointed-end-capping ability of Lmod2$_{1-514}$. Pointed-end polymerization of actin filaments saturated with Tpm1.1 (1.25 μM for WT or 2 μM for R21H) in the absence (A) or presence (B) of 10 nM Lmod2$_{1-514}$ was monitored. (C) Dependence of the pointed-end capping effect on Lmod2$_{1-514}$ concentration in the presence of Tpm1.1. Inhibition of pointed-end actin polymerization by Lmod2$_{1-514}$ was quantified as $R_{exp}/R_{control}$ values. Initial rates (R) were determined as the first derivatives at time 0 of polymerization curves after exponential fitting. (D) Inhibition of actin polymerization in the presence of 10 nM Lmod2. Asterisks demonstrate statistically significant differences between groups (**$p < 0.01$) using one-way ANOVA with Holm-Sidak post-hoc test. Standard deviations are indicated as error bars ($n = 3$–4).

Next, we investigated whether the Tpm1.1 mutations affect Lmod2-induced bundle formation. At 4000 × g, we detected a higher amount of pelleted actin when Tpm1.1[R21H] was present than those in the presence or absence of WT Tpm1.1 (Figure 8), indicating that Tpm1.1[R21H] induces heavier bundles. In the presence of Tpm1.1[K15N], the amount of pelleted actin at 4000 × g was reduced compared with when only Lmod2 was present.

We used TEM to visualize F-actin bundles formed in the presence of Tpm1.1[R21H]. In the presence of Tpm1.1[R21H], Lmod2 packs F-actin into dense bundles (Figure 7D), where actin filaments demonstrate arrangement different from that observed in the presence of WT Tpm1.1 (Figure 7D, insert). Formation of thicker and more densely packed bundles in the presence of Tpm1.1[R21H] is consistent with our cosedimentation data (Figure 8) because thicker bundles should sediment more efficiently at 4000 × g than thinner bundles. There was no difference in the Lmod2/actin ratio in precipitated filaments, and, therefore, the difference in the bundle formation suggests that the R21H mutation affects the mode of binding of Lmod2 along the side of Tpm-saturated F-actin.

DISCUSSION

Effects of both mutations on the N-terminal structure of Tpm1.1 are characterized in previous studies (Colpan *et al.*, 2016b; Ly *et al.*, 2018). While both mutations decrease the α-helical content of Tpm1.1 near its N-terminus, the R21H mutation results in a more pronounced structural effect: it causes a ~60% reduction in the helical content of αTm1a$_{1-28}$Zip, a chimeric peptide containing the first 28 residues of Tpm1.1 and significantly decreases the peptide's thermal stability (Ly *et al.*, 2018). Residues Lys-15 and Arg-21 are located near the overlap region between Tpm1.1 molecules which spans ~11–15 residues (Greenfield *et al.*, 2006; Frye *et al.*, 2010) and interacts with ~39 residues within the N-terminal region of cTnT (Pearlstone and Smillie, 1977; Jin and Chong, 2010). This cTnT-Tpm overlap complex is physiologically important. Many cardiomyopathy-linked mutations in the N-terminus of cTnT that binds to the Tpm overlap have been identified (Palm *et al.*, 2001; Hershberger *et al.*, 2009). The C-terminus of cTnT interacts with the N-terminal domain of cTnI and C-terminal globe of cTnC, integrating cTnT into the core domain of cTn (Takeda *et al.*, 2003). Since both mutations alter the local N-terminal conformation of Tpm1.1, the mutations may produce structural effects that spread through the cTnT-binding overlap region to cTn, altering normal structural arrangements within cTn.

FRET has been used to study structural changes within cTn in many studies, including those involving IAEDANS and DDPM probes attached to residue 151 or 167 or cTnI and residue 89 of cTnC, respectively (Robinson *et al.*, 2004; Ouyang *et al.*, 2010;

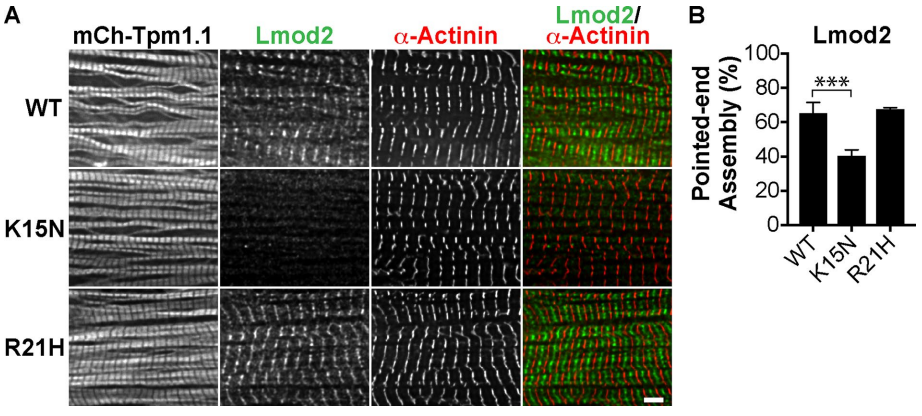

FIGURE 6: Assembly of Lmod2 at the pointed end of the thin filament is reduced in cells expressing Tpm1.1[K15N]. (A) Representative images of rat neonatal cardiomyocytes expressing mCherry-tagged WT Tpm1.1, Tpm1.1[K15N], or Tpm1.1[R21H] stained with an antibody to Lmod2 (green) and an antibody to α-actinin (red). Scale bar = 3 μm. (B) Mean percentage of cells with thin-filament pointed-end assembly of Lmod2 ± SD ($n = 3$ cultures). A one-way ANOVA with Dunnett's post-hoc test was used to compare each mutant to WT (***$p < 0.001$).

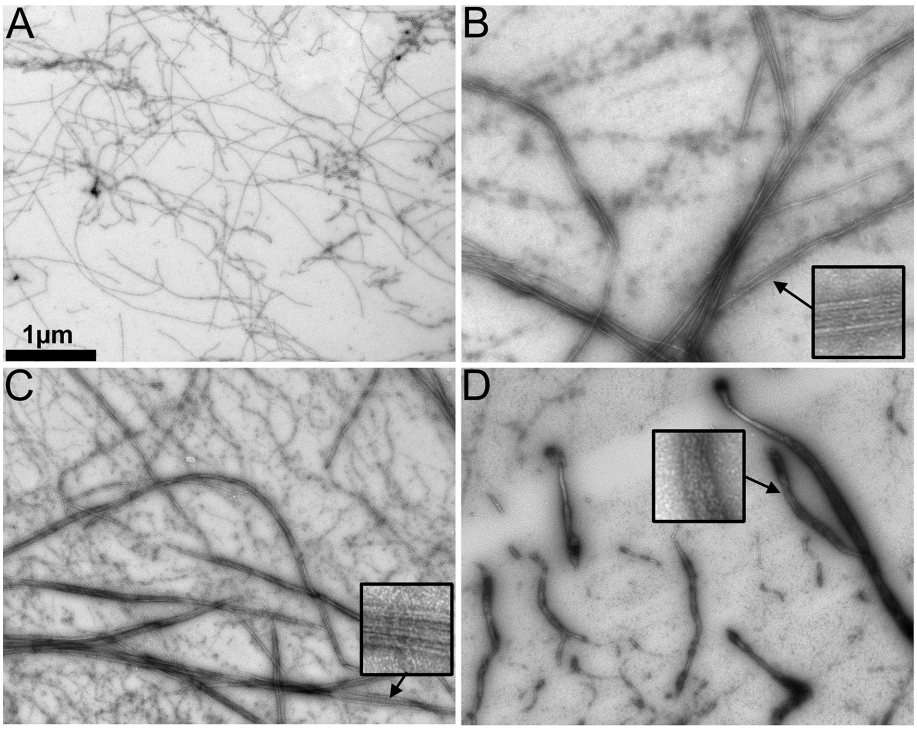

FIGURE 7: TEM images of negatively stained actin filaments in the absence (A) and presence (B–D) of Lmod2. F-actin (A) forms bundles in the presence of Lmod2 in the absence of Tpm1.1 (B) or in the presence of WT Tpm1.1 (C) or Tpm1.1[R21H] (D). Inserts show different packing of actin filaments within Lmod2 induced bundles. Bar is 1 μm.

Schlecht *et al.*, 2014). In this study, time-resolved fluorescence decay measurements show that the K15N mutation in Tpm1.1 increases mean interprobe distances when thin filaments are under a free-Ca^{2+} condition or under a high-Ca^{2+} condition, while the R21H mutation does not affect these distances. These data suggest that the K15N mutation cause alteration of normal structural arrangements within cTn core domain, specifically the relative positions of N-cTnC and cTnI-R. In addition to the cTnT-binding overlap region between Tpm1.1 molecules, the K15N mutation in Tpm1.1 may exert such structural effects on the cTn core domain through another site in Tpm1.1 that binds to ~25-residue region near the beginning of the C-terminal domain of TnT (Jin and Chong, 2010). The orientation of cTnT on the thin filament is still under debate (Ohtsuki, 1979; Pirani *et al.*, 2006; Paul *et al.*, 2009, 2017; Yang *et al.*, 2014). Although it is clear that the N-terminus of cTnT extends from the core domain of cTn and makes contact with the Tpm overlap region, the structure of the N-terminus of cTnT with the Tpm overlap is not agreed on (Greenfield *et al.*, 2006; Murakami *et al.*, 2008; Frye *et al.*, 2010). It is possible that Lys-15 in Tpm1.1 is within the binding site to cTnT or affects binding to cTnT by disturbing the overlap region while Arg-21 is not. This would explain why more drastic structural changes in Tpm1.1 caused by the R21H mutation have very little effect on cTn.

Ca^{2+} titration experiments show that the K15N mutation in Tpm1.1 decreases the thin filament's sensitivity to Ca^{2+}, whereas the R21H mutation has almost no effect (Table 2). The effects of the K15N and R21H mutations in Tpm1.1 on the ATPase rates are in agreement with Ca^{2+} titration experiments. The K15N mutation therefore can join a growing list of DCM-linked mutations in thin-filament regulatory proteins that reduce Ca^{2+} affinity of cardiac thin filaments (Mirza *et al.*, 2005, 2007; Borovikov *et al.*, 2009).

Decreased myofilament Ca^{2+} sensitivity has been identified as an important factor leading to DCM caused by thin-filament-associated mutations, and early sensitization of myofilaments to Ca^{2+} may be used as a therapeutic target to treat thin-filament-linked DCM (Du *et al.*, 2007; Alves *et al.*, 2017). In general, cardiomyopathy-linked Tpm mutations can exert different effects on thin-filament regulation, and these effects could be carried along the thin filament through changes in Tpm's position on actin, through cTn, and through alterations of actomyosin interactions (Redwood and Robinson, 2013). The effect of the K15N mutation on the core domain of cTn observed in this study could be carried through cTnT, leading to alteration of cTn's binding to actin. More specifically, cTn is known to bind to actin in the core domain at cTnI-I, cTnI-M and part of cTnT (Rieck and Dong, 2014). The reduction in Ca^{2+} sensitivity caused by the K15N mutation may be explained by the observed increase in the mean interprobe distance, since the probability of cTnI-R interacting with the hydrophobic pocket of N-cTnC is reduced when they are farther apart. In addition to the decreased Ca^{2+} sensitivity, the K15N mutation results in a decrease in I_R-C_N dissociation rate triggered by the removal of Ca^{2+} from N-cTnC. As thin filaments switch from being under a high-Ca^{2+} condition to being under a free-Ca^{2+} condition, misalignment of cTnI-I and cTnI-M with respect to their target sites on actin could lead to a longer duration in which they randomly diffuse, after dissociating from cTnC, before binding to actin. Therefore, it is possible that the K15N mutation affects the structure of the core domain of cTn both by bringing cTnI-R out of its normal alignment with N-cTnC and by changing the normal orientation of cTnI-I and cTnI-M with their respective binding sites on actin. These possible structural alterations within the cTn core domain are demonstrated as a schematic representation (Supplemental Figure S6), which is based on a previously proposed model for Tn activation and relaxation (Vinogradova *et al.*, 2005). This would explain the increased mean interprobe distances when thin filaments are under a free-Ca^{2+} condition or under a high-Ca^{2+} condition, reduced Ca^{2+} sensitivity of thin filaments and decreased I_R-C_N dissociation kinetics as a consequence of the K15N mutation in Tpm1.1.

In this study, for the first time, the bundling of F-actin induced by side-binding Lmod2 is visualized using TEM. Formation of F-actin bundles in the presence of Lmod2 was confirmed using cosedimentation (Figure 8). We also showed that the Tpm1.1 mutations have opposite effects on the degree of F-actin bundling. Using both cosedimentation and TEM, we demonstrated that the R21H mutation in Tpm1.1 induces thicker and more densely packed F-actin bundles, which implies that the mutation changes how Lmod2 associates with the sides of F-actin. Both mutations reduce Tpm1.1's affinity for F-actin: we observe a twofold decrease for the R21H mutant and a threefold decrease for the K15N mutant (Colpan *et al.*, 2017). We suggest that changes in Tpm1.1's affinity for F-actin caused by the mutations impose different effects on Tpm1.1's

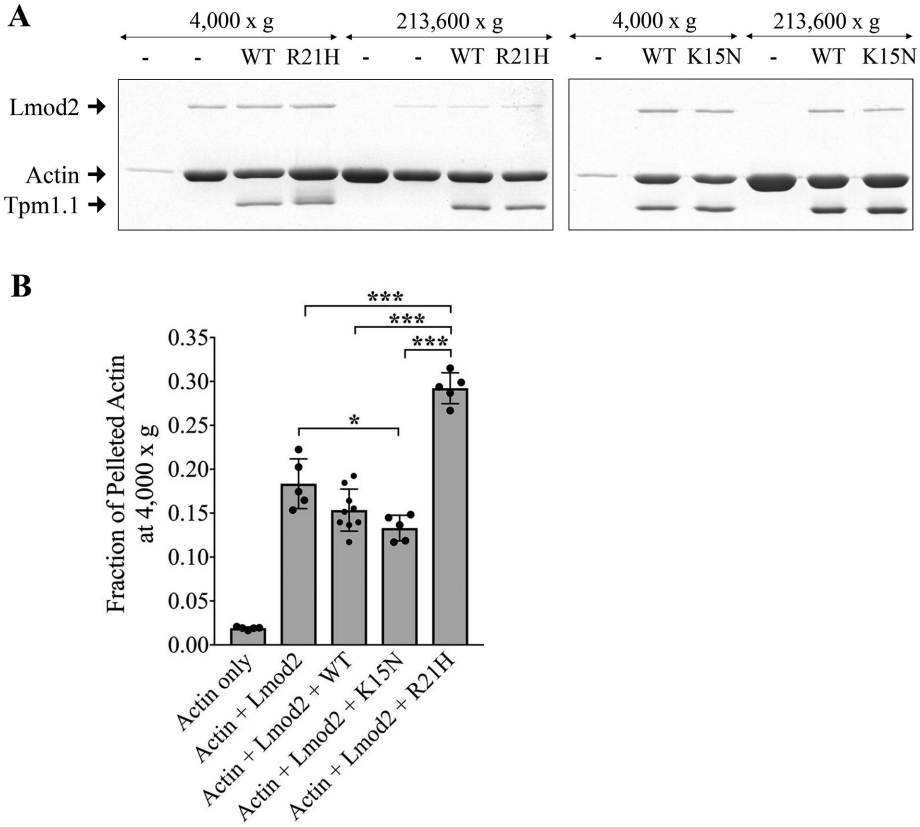

FIGURE 8: Separation of F-actin bundles induced by Lmod2 side binding using centrifugation. F-actin (4 μM) was mixed with saturating concentrations of Tpm1.1 (1.25 μM for WT or 2 μM for R21H) and 0.9 μM Lmod2 in 2 mM Tris–HCl, pH 8.0, 25 mM imidazole, 100 mM KCl, 2 mM $MgCl_2$, 1 mM EGTA, 0.2 mM $CaCl_2$, 0.01% NaN_3, 0.5 mM DTT, and 0.5 mM ATP. (A) A representative image of the SDS–PAGE of pellets after centrifugation. (B) Fractions of pelleted actin were calculated by dividing band densities of actin pelleted at 4000 × *g* by those of the corresponding total pelleted actin. Averages and standard deviations of the data ($n = 5$–9) are demonstrated by columns and error bars, respectively. Asterisks demonstrate statistically significant differences between groups (*$p < 0.05$, ***$p < 0.001$) using one-way ANOVA with Holm-Sidak post-hoc test.

binding to F-actin and in turn alter Lmod2's binding to the sides of F-actin.

We have previously demonstrated that the K15N mutation decreases the binding affinity of αTM1a$_{1\text{-}21}$Zip, a chimeric peptide containing 21 N-terminal residues of Tpm1.1, for Tmod1s1, Tmod1s2, and Lmod2s1 peptides (Colpan *et al.*, 2016b, 2017). As a result, the K15N mutation reduces the ability of Lmod2$_{1\text{-}514}$ and Tmod1 to inhibit pointed-end polymerization (Colpan *et al.*, 2017). In this study, we detected a reduction in thin-filament pointed-end assembly of Lmod2 following expression of Tpm1.1[K15N] in rat neonatal cardiomyocytes (Figure 6), whereas the pointed-end assembly of Tmod1 was found to be normal in these cells. It is possible that there is a connection between the reduced Lmod2-induced F-actin bundling in the presence of Tpm1.1[K15N] (Figure 8) and the decrease in Lmod2's pointed-end assembly in cardiomyocytes. Future high-resolution structural studies showing how full-length Lmod2 interacts with F-actin will elucidate if there is such a connection.

Expression of mCherry-tagged Tpm1.1 constructs in rat neonatal cardiomyocytes allows for detection of the Tpm1.1 mutants in cardiomyocytes. Since the mCherry tag is located at the N-terminus of Tpm1.1, which is close to the Tpm overlap region, the tag may interfere with Tpm1.1 function. However, it was shown that N-terminal tagged-Tpm1.1 assembles along the length of the thin filament and is excluded from the Z-disk, which mimics the assembly of endogenous Tpm (Helfman *et al.*, 1999). Furthermore, cells expressing tagged-Tpm1.1 have sarcomeres which shorten and appear to contract normally. These observations suggest the introduction of a fluorescent tag on Tpm1.1, as well as its overexpression, do not significantly compromise the function of Tpm1.1 or calcium-activated contraction.

Characterization of mutations in Tpm1.1 and other thin-filament regulatory proteins requires an understanding of the mutations' effects not only on the structure and function of the affected protein but also on those of its binding partners. The data presented in this study and those from other studies that were discussed provide more insights into the disease-causing mechanisms by mutations in Tpm1.1. We demonstrated that the Tpm1.1 mutations linked to different cardiomyopathies have different effects on the functions of Tpm1.1's binding partners. On the basis of our data, we suggest that the K15N mutation causes DCM mainly by altering the Ca^{2+}-dependent thin-filament regulation. Data obtained for the R21H mutation shed light on possible mechanisms underlying development of HCM. Knowing how cTn orients on the thin filament and the mode of binding of Lmod2 on the filament will significantly contribute to the understanding of disease mechanisms.

MATERIALS AND METHODS

Protein sequences

Tpm1.1 (NP_001288265.1), cTnI (NP_058840.1), cTnC (NP_001029277.1), cTnT (NP_036808.1), Tmod1 (NP_990358.1), and Lmod2 (NP_001186644.2 for Lmod2$_{1\text{-}514}$, NP_444328.1 for full-length Lmod2) sequences were obtained from the NCBI website.

Plasmid construction and site-directed mutagenesis

Recombinant full-length Tpm1.1 has an N-terminal extension consisting of two residues Ala-Ser to mimic the native N-terminal acetyl group (Monteiro *et al.*, 1994). The K15N and R21H mutations were individually introduced into full-length WT Tpm1.1 using site-directed mutagenesis as previously described (Colpan *et al.*, 2016b; Ly *et al.*, 2018). To facilitate fluorophore labeling of cTnI and cTnC for FRET experiments in this study, single-cysteine mutants cTnI[S151C], cTnI[S167C], and cTnC[S89C] were generated through two steps of site-directed mutagenesis starting with plasmid templates encoding WT rat cTnI and cTnC as previously described (Xing *et al.*, 2009; Zhou *et al.*, 2012; Schlecht *et al.*, 2014).

Full-length Lmod2 was cloned from cDNA generated from a neonatal mouse cardiomyocyte culture. A single alanine (GCA) was added to the C-terminus of Lmod2 (for efficient dithiothreitol

[DTT]-induced cleavage) and inserted into pTYB3 (New England BioLabs, Ipswich, MA) between *Nco*I and *Sap*I (blunted) restriction sites, which fuses an intein-tag to the C-terminus of Lmod2. The inserted sequence was confirmed by DNA sequencing, and the expression construct transformed into *Escherichia coli* BL21-Codon Plus (DE3)-RIPL competent cells (Agilent Technologies, Santa Clara, CA).

Expression construct of rat Tpm1.1 was a gift from J. C. Perriard (Eidgenössische Technische Hochschule Zürich, Zürich, Switzerland). The sequence for Tpm1.1 was cloned into a modified pEGFP-C2 vector (Clontech, Moutain View, CA) in which GFP was replaced with mCherry. The K15N and R21H mutations were introduced to mCherry-tagged Tpm1.1 via site-directed mutagenesis using the following primer sequences: K15N (forward: 5′-CTCGACAATGAGAACGCCTTGGATCGAGCAGAG and reverse: 5′-AGAAGATGCAGATGCTGAAGCTCGACAATGAGA ACG); R21H (forward: 5′-TTGGATCACGCAGAGCAGGCGGAG-GCTGACAA and reverse: 5′-CTCTGCGTGATCCAAGGCGTT-CTCTTTGTCGAG-) (Liu and Naismith, 2008). All sequences were confirmed by DNA sequencing.

Protein expression, purification, and labeling

Tpm1.1 (WT or mutants) was expressed in *E. coli* BL21 (DE3) and purified as previously described (Colpan *et al.*, 2016a). G-actin was purified as described in Ly *et al.* (2016). G-actin was labeled with *N*-(1-pyrene)iodoacetamide as previously reported (Kouyama and Mihashi, 1981; Cooper *et al.*, 1983) and stored in liquid nitrogen. Prior to pointed-end capping experiments, pyrene iodoacetamide-labeled actin was thawed and centrifuged at 70,000 rpm (TLA-120.1 rotor; Beckman Coulter, Brea, CA) and 4°C for 30 min to remove aggregates.

All recombinant cardiac troponin proteins were expressed and purified as previously described (Guo *et al.*, 1994; She *et al.*, 1998; Dong *et al.*, 2001). Mutations introduced to WT cTnI and cTnC to create single cysteine mutants were found to have minimal effects on the functions of Tn (Dong *et al.*, 1997b, 2001; Robinson *et al.*, 2004; Xing *et al.*, 2009; Zhou *et al.*, 2012). Each single cysteine cTnI mutant was modified with IAEDANS to be used as FRET donor, and cTnC[S89C] was labeled with DDPM as FRET acceptor according to previously reported procedures (Robinson *et al.*, 2004). The labeling ratios were all greater than 95%, which was determined using spectroscopy with ε_{325} = 6000 $cm^{-1}M^{-1}$ for IAEDANS and ε_{442} = 2930 cm^{-1} M^{-1} for DDPM as in Schlecht *et al.* (2014). Myosin subfragment-1 (S1) was isolated by conducting chymotrypsin digestion of myosin purified from rabbit skeletal muscle (Xing and Cheung, 1994). Actin used in FRET experiments was prepared from rabbit skeletal muscle and purified as in Ly *et al.* (2016).

Tmod1 was expressed and purified as previously described (Kostyukova *et al.*, 2000). $Lmod2_{1\text{-}514}$ was purified according to Tsukada *et al.* (2010). Expression of Lmod2 was done with 0.4 mM IPTG in LB broth and shaking at room temperature for 4 h. Cells were collected by centrifugation (4000 × *g*, 15 min, 4°C). Pellets were resuspended in B-PER Bacterial Protein Extraction Reagent (Thermo Fisher Scientific, Waltham, MA) + DNase and Halt protease inhibitor cocktail (Thermo Fisher Scientific) and incubated for 15 min at room temperature followed by 15 min on ice. Column buffer (50 mM Tris–HCl, pH 8.5, 500 mM NaCl, 1 mM EDTA, 0.2% Tween + protease inhibitor cocktail) was added, and the cells were sonicated on ice. Clarified extract (spun at 15,000 × *g*, 25 min, 4°C) was added to a column of chitin resin (New England BioLabs). Following washes with column buffer, self-cleavage was induced by overnight incubation in cleavage buffer (50 mM Tris–HCl, pH 8.5, 500 mM NaCl, 1 mM EDTA, 50 mM DTT) at 4°C. The cleavage resulted in tagless Lmod2 with no extraneous sequence. Following elution, proteins were exchanged into 20 mM Tris–HCl, pH 8.0, 50 mM KCl, 2 mM $MgCl_2$.

Recombinant human gelsolin was a gift from John Hartwig (Brigham and Women's Hospital, Boston, MA). Protein purity was determined using SDS–PAGE. Protein concentrations were determined by either using a BCA protein assay kit (Thermo Fisher Scientific) or measuring the difference between their absorptions at 294 nm at pH 7.0 and pH 12.5 in 6 M guanidine hydrochloride using difference extinction coefficients of 2357 cm^{-1} per 1 M tyrosine and 830 cm^{-1} per 1 M tryptophan (Edelhoch, 1967; Fasman, 1989).

Cardiac thin-filament reconstitution

Actin, Tpm1.1 (WT or mutants), wild-type cTnT, labeled cTnI and cTnC were reconstituted into thin filaments using a cTn:Tpm1.1:actin molar ratio of 1:1.1:7 as previously described (Zhou *et al.*, 2012; Schlecht *et al.*, 2014). Briefly, following the stepwise dialysis to remove urea, salt concentration was gradually reduced from 0.5 to 0.4, 0.3, 0.25, and 0.2 M KCl in the reconstitution buffer containing 30 mM 3-(*N*-morpholino)propanesulfonic acid (MOPS), pH 7.0, 5 mM $MgCl_2$, 1 mM ethylene glycol-bis(2-aminoethylether)-*N*,*N*,*N*′,*N*′-tetraacetic acid (EGTA), and 1 mM DTT. F-actin and Tpm1.1 (WT or mutants) were combined with the cTn complex at the dialysis step with 0.3 M KCl. After the dialysis step in 0.2 M KCl reconstitution buffer, thin filaments were dialyzed against the titration buffer containing 0.2 M KCl, 50 mM MOPS, pH 7.1, 5 mM nitrilotriacetic acid (NTA), 5 mM $MgCl_2$, 2 mM EGTA, and 1 mM DTT for Ca^{2+} titration and fluorescence lifetime experiments. For stopped-flow experiments, the samples were dialyzed against a buffer containing 0.2 M KCl, 40 mM MOPS, pH 7.0, 5 mM $MgCl_2$, 10 µM EGTA, and 1 mM DTT. For all the experiments, myosin S1 was dialyzed against the same buffer as the final buffer of the samples. Immediately before each experiment, 3 µM S1 and 5 mM ADP were added to 1 µM thin filaments. ADP-bound myosin is known to bind strongly to actin (Lymn and Taylor, 1970, 1971; Sweeney and Houdusse, 2010; Wulf *et al.*, 2016). All Ca^{2+} titrations, lifetime, and stopped-flow experiments were conducted within 3–5 d following reconstitution to prevent sample degradation.

Steady-state Ca^{2+} titration fluorescence measurements

Measurements were carried out at 15 ± 0.1°C on an ISS PCI photon counting spectrofluorimeter equipped with a microtitrator. Prior to each measurement, appropriate buffer dilutions were made to reduce the KCl concentration to 0.15 M, while the rest of the buffer components remained the same (50 mM MOPS, pH 7.1, 5 mM NTA, 5 mM $MgCl_2$, 2 mM EGTA, and 1 mM DTT). The fluorescence intensity of the donor (cTnI[S151$C_{IAEDANS}$] or cTnI[S167$C_{IAEDANS}$]) was monitored at 488 nm with excitation at 335 nm. In each titration, aliquots of 3 µl of 14 mM Ca^{2+} solution were successively injected into 1.2 ml of the reconstituted thin-filament sample in the presence or absence of myosin S1. Adjusted fluorescence intensities were calculated from the experimental data to account for the effect of dilution on the fluorescence signal. The intensities were normalized and plotted against free-Ca^{2+} concentrations that were determined using an in-house program, with stability constants provided by Fabiato (1988). Titration data were fitted to the Hill equation as in Schlecht *et al.* (2014) to obtain pCa_{50}, which is the midpoint of the titration or the half-maximal thin-filament activation, using SigmaPlot 12.5 (Systat Software, San Jose, CA):

$$I = (I_{max} - I_{min}) \frac{\left[Ca^{2+}\right]^{n_H}}{\left[Ca^{2+}\right]^{n_H} + 10^{-pCa_{50}}} + I_{min}$$

where I is the steady-state donor fluorescence intensity, I_{max} and I_{min} correspond to the donor intensity under Ca^{2+}-free and Ca^{2+}-saturated conditions, respectively, and n_H is the Hill coefficient.

Time-resolved fluorescence measurements

TCSPC fluorescence decay of the donor (cTnI[S151$C_{IAEDANS}$] or cTnI[S167$C_{IAEDANS}$]) in the absence or presence of the acceptor (cTnC[S89C_{DDPM}]) was monitored under the same buffer conditions as used in Ca^{2+} titration experiments. Measurements were conducted on a FluoreCube time-correlated single-photon counting system (HORIBA Jobin Yvon, Edison, NJ) as previously described (Schlecht *et al.*, 2014). Time-resolved fluorescence decays were fitted with multiexponential functions as previously discussed (Dong *et al.*, 1997a; Schlecht *et al.*, 2014) using the DecayFit 1.4 software. Fluorescence decay fitting yielded a distribution of interprobe distances along with fitting parameters $\overline{r}$, which is the mean interprobe distance or the distance corresponding to the peak of the distribution, and the FWHM of the distribution.

Stopped-flow fluorescence measurements

Measurements were conducted at 6.0°C using a T-format KinTek stopped-flow spectrometer with a 1.8-ms dead time. Prior to each measurement, appropriate buffer dilutions were made to reduce the KCl concentration to 0.15 M, while the rest of the buffer components remained the same (40 mM MOPS, pH 7.0, 5 mM $MgCl_2$, 10 µM EGTA, and 1 mM DTT). In each measurement, Ca^{2+}-saturated reconstituted cardiac thin filaments were rapidly mixed with an equal volume of buffer containing an excess amount of BAPTA, a strong Ca^{2+}-specific chelator. Change in the fluorescence intensity of the donor (cTnI[S151$C_{IAEDANS}$] or cTnI[S167$C_{IAEDANS}$]) was recorded within 0.3 s. Up to 20 traces were obtained for each set of samples, and the average trace was fitted to an exponential function to determine the rate constant of the conformational change induced by the dissociation of Ca^{2+} from cTnC.

Cosedimentation of Tpm1.1 with F-actin

Prior to each cosedimentation experiment, Tpm1.1 was reduced by adding 2 mM DTT, heating for 5 min at 56°C, and aggregates were removed by centrifuging for 30 min at 65,000 rpm (Beckman Coulter TLA-120.1 rotor) and 20°C. Cosedimentation assays to quantify the affinity of Tpm1.1 (WT or R21H) to F-actin were conducted according to a recently published protocol (Colpan *et al.*, 2017) with minor changes: 0–3 µM Tpm1.1 (WT or R21H) was used, and the F-actin/Tpm1.1 mixture was incubated for 10 min at room temperature before centrifugation. The data were fitted to both the Hill equation (Barua *et al.*, 2011) using SigmaPlot 12.5 and the McGhee–von Hippel equation (McGhee and von Hippel, 1974), corrected in Leinweber *et al.* (1999), using Prism 7.0 (GraphPad Software, La Jolla, CA). Fitting the data to the Hill equation yielded $K_{app,}$ which is the apparent binding constant between Tpm1.1 and actin:

$$f = \frac{a \times c^n \times K_{app}^n}{1 + c^n \times K_{app}^n}$$

where f is the fraction maximal Tpm1.1 binding to actin or the normalized Tpm1.1/actin band density ratio, a is the maximal bound Tpm1.1, c is the free-Tpm1.1 concentration, and n is the Hill coefficient. Analysis using the McGhee–von Hippel model determined K_o, which is the binding constant between Tpm1.1 and an isolated binding site on F-actin:

$$\frac{v}{L} = K_o \times (1 - n \times v) \times \left(\frac{(2 \times \omega - 1) \times (1 - n \times v) + v - R}{2 \times (\omega - 1) \times (1 - n \times v)} \right)^6 \times \left(\frac{1 - (n+1) \times v + R}{2 \times (1 - n \times v)} \right)^2$$

where $R = \sqrt{(1 - (n+1) \times v)^2 + 4 \times \omega \times v \times (1 - n \times v)}$, v is the number of moles of bound Tpm1.1 per mole of actin, L is the free-Tpm1.1 concentration, n the stoichiometry of actin to bound Tpm1.1 (hence, $n = 7$), and ω is the increase in Tpm1.1s affinity for a contiguous binding site (an end-to-end contact with an adjacent molecule).

ATPase assays

Rates of ATP hydrolysis were measured by the time course of liberation of ^{32}Pi from [γ-^{32}P]ATP on addition of myosin S1 (Chalovich and Eisenberg, 1982). The total reaction volume was 0.4 ml, and 0.1 ml aliquots of the reaction mixture were analyzed at 4, 8, and 12 min. All reactions were linear over that period and the initial rate was determined by a linear least-squares fit of the data. Measurements were taken at 25°C with 0.1 µM skeletal myosin S1, 10 µM F-actin, 2.9 µM Tpm (WT or mutated), and 2.9 µM human cTn. The assay solution contained 1 mM ATP, 3 mM $MgCl_2$, 34 mM NaCl, 10 mM MOPS, pH 7.0, and 1 mM DTT, with 2 mM EGTA or 0.2 mM $CaCl_2$.

Fluorescence measurements of pointed-end polymerization

The rate of actin polymerization was measured as the change in pyrene-labeled actin fluorescence using a PTI Quantmaster Model QM-40 Spectrofluorometer (HORIBA Scientific, Edison, NJ) (excitation at 366 nm, emission at 387 nm, 2-nm slit width) according to Kostyukova and Hitchcock-DeGregori (2004). To measure the inhibition rates of actin polymerization at the pointed ends by Tmod1 or $Lmod_{1\text{-}514}$, actin seeds (short actin filaments whose barbed ends are capped by gelsolin) were prepared by polymerizing 3 µM G-actin in the presence of 30 nM gelsolin at room temperature for at least 1 h. Next, saturating concentrations of Tpm1.1 (1.25 µM for WT or 2 µM for R21H) was added to the seeds and incubated for 1–2 min before 0–50 nM Tmod1 or 0–40 nM $Lmod2_{1\text{-}514}$ was added to the Tpm1.1-saturated actin seeds. The seeds were diluted five times with 1 µM G-actin and 0.1 µM pyrene actin in 2 mM Tris–HCl, pH 8.0, 25 mM imidazole, 100 mM KCl, 2 mM $MgCl_2$, 1 mM EGTA, 0.2 mM $CaCl_2$, 0.01% NaN_3, 0.5 mM DTT, and 0.2 mM ATP. The data were fitted to an exponential growth to maximum equation using SigmaPlot 12.5. The initial rates (R) of polymerization were calculated as the first derivatives of the exponential curves at time 0. $R_{exp}/R_{control}$ was calculated as the normalized inhibition of pointed-end polymerization by Tmod1 or $Lmod2_{1\text{-}514}$, where $R_{control}$ is the rate of pointed-end actin polymerization without any Tpm1.1, Tmod1, or $Lmod2_{1\text{-}514}$.

Isolation, transduction, and immunofluorescence microscopy of neonatal cardiomyocytes

Rat neonatal cardiomyocytes were isolated and plated on matrigel thin-coated (BD Biosciences, Franklin Lakes, NJ), 12-mm glass coverslips placed in culture dishes as previously described (Pappas *et al.*, 2015). One day after plating, cells were transduced with 20 multiplicity of infection (MOI) of mCherry-tagged rat Tpm1.1, Tpm1.1[K15N], or Tpm1.1[R21H] adenovirus, which were generated as previously described (Pappas *et al.*, 2015). The mCherry tag is located at the N-terminus of Tpm1.1. At 20 MOI, all cells express the tagged proteins.

Four days after transduction, cells were washed with phosphate-buffered saline (PBS) and incubated in relaxing buffer (150 mM KCl, 5 mM $MgCl_2$, 10 mM 3-(*N*-morpholino)propanesulfonic acid, pH 7.4, 1 mM EGTA, and 4 mM ATP) for 15 min and fixed with 2% (wt/vol) paraformaldehyde in relaxing buffer for 15 min. Cells were then permeabilized in 0.2% Triton X-100/PBS for 20 min at room temperature, blocked with 2% bovine serum albumin (BSA) plus 1% normal donkey serum/PBS for 1 h at room temperature, and incubated 1–4 h at room temperature with primary antibodies/PBS, which included mouse monoclonal anti-α-actinin (1:200) (EA-53; Sigma-Aldrich, St. Louis, MO), rabbit polyclonal anti-Tmod1 (2 µg/ml), and rabbit polyclonal anti-Lmod2 (1 µg/ml) (E-13; Santa Cruz Biotechnology, Dallas, TX). Cells were then washed with PBS for 20 min and incubated for 1.5 h at room temperature with secondary antibodies/PBS, which included Alexa Fluor 405-conjugated goat anti-mouse immunoglobulin G (IgG) (1:200) (Thermo Fisher Scientific) and Alexa Fluor 647-conjugated donkey anti-rabbit IgG (1:600) (Jackson ImmunoResearch Laboratories, West Grove, PA). Cells were washed with PBS for 20 min then mounted onto slides with Aqua Poly/Mount (Polysciences, Warrington, PA) or ProLong Diamond Antifade Mountant (Thermo Fisher Scientific). Images were captured using a Nikon Eclipse T*i* microscope with a 100 × NA 1.5 objective, and a digital complementary metal oxide semiconductor (CMOS) camera (ORCA-flash4.0; Hamamatsu Photonics, Shizuoka Prefecture, Japan). Images were deconvolved using NIS offline deconvolution software (Nikon Corporation, Tokyo, Japan) and processed using Photoshop CC (Adobe, San Jose, CA). Cells were considered to have thin-filament pointed-end assembly of Lmod2/Tmod1, if a clear striation was visible in the majority of sarcomeres within the cell.

Immunoblots

To determine the amount of assembled Tpm, cell lysate collected from the same culture dishes as those used for immunofluorescence microscopy (after coverslips were removed) was fractionated. Briefly, cells were rinsed twice with ice-cold PBS, and then the cytosol extracted in a Triton X-100–containing cytoskeleton stabilization buffer (CSK: 10 mM PIPES, pH 6.8, 100 mM KCl, 300 mM sucrose, 2.5 mM $MgCl_2$, 1% Triton X-100 plus protease inhibitors) for 5 min on ice while rocking. After two 5-min washes on ice with CSK buffer without Triton X-100, the cells were quickly rinsed twice with PBS. The cells were then collected in 2x Laemmli buffer with a cell scraper, briefly sonicated and incubated at 100°C for 10 min. Lysate was resolved on 10% SDS gels and transferred to a nitrocellulose membrane (0.2 µm pore size; Amersham Protran, GE Healthcare, Little Chalfont, United Kingdom). Following transfer, the membrane was blocked with 5% (wt/vol) nonfat dried milk/TBS for 1 h at room temperature and then incubated with primary antibodies in 1% BSA (wt/vol)/Tris-buffered saline with 0.1% Tween20 (TBST) overnight at 4°C. Primary antibodies included mouse monoclonal anti-Tpm (1:2000) (TM311; T2780; Sigma-Aldrich) and a goat polyclonal anti-α-actinin (0.4 µg/ml) (N19; sc-7453, Santa Cruz Biotechnology). The membranes were then washed five times, each for 5 min in TBST and incubated with fluorescently labeled anti-rabbit or anti-goat IgG (1:40,000) (Jackson ImmunoResearch) diluted in 5% milk/TBST for 1 h at room temperature. Blots were imaged and analyzed using a LI-COR Odyssey CLx imaging system (LI-COR Biosciences, Lincoln, NE).

Transmission electron microscopy imaging

G-actin (4 µM) was incubated in 0.4 mM ATP, 2 mM Tris, pH 7.5, 0.2 mM $CaCl_2$, 0.01% NaN_3, and 0.5 mM DTT for 10 min on ice. Polymerization buffer (20X) was added to G-actin to reach a final concentration of 1X (100 mM KCl, 25 mM imidazole, pH 8.0, 2 mM $MgCl_2$, 1 mM EGTA, and 0.1 mM ATP), and actin was polymerized for 30 min at room temperature. F-actin was kept at 4°C for several hours during TEM imaging. From the same batch of prepared F-actin, all TEM samples (including the actin-only control) were prepared. Wild-type Tpm1.1 (1.25 µM) or 2 µM Tpm1.1[R21H] was added to F-actin and the mixture was incubated at 4°C for 10 min. Lmod2 (0.9 µM) was added to F-actin in the absence or presence of Tpm1.1 and incubated at room temperature for 10 min.

To visualize complexes of F-actin with Lmod2 and with or without bound Tpm1.1, aliquots (7 µl) were applied to glow-discharged carbon-coated grids (Electron Microscopy Sciences, Hatfield, PA) and stained with 2% uranyl acetate. The grids were examined in a JEOL 1200 EXII transmission electron microscope (JEOL USA, Peabody, MA) under regular dose conditions at an accelerating voltage of 70 keV.

Pellet samples from cosedimentation assays were run on 10% polyacrylamide SDS gels. The gels were scanned using ChemiDoc XRS (Bio-Rad, Hercules, CA) and quantified using the National Institutes of Health ImageJ software.

ACKNOWLEDGMENTS

We thank Joseph Chalovich for discussion on ATPase assays, Nazanin Bohlooli Ghashghaee for her help with the DecayFit software, and Rachel Mayfield for help with neonatal rat cardiomyocyte cultures. This study was supported by National Institutes of Health (NIH) Grant GM120137 to Alla Kostyukova and Carol Gregorio and Grant R01HL123078 to Carol Gregorio. Thu Ly was supported by American Heart Association Predoctoral Fellowship 17PRE33680008 and in part by the NIH/National Institute of General Medical Sciences–funded protein biotechnology training program T32 GM008336 to Washington State University.

REFERENCES

Alves ML, Warren CM, Simon JN, Gaffin RD, Montminy EM, Wieczorek DF, Solaro RJ, Wolska BM (2017). Early sensitization of myofilaments to Ca2+ prevents genetically linked dilated cardiomyopathy in mice. Cardiovasc Res 113, 915–925.

Barua B, Pamula MC, Hitchcock-DeGregori SE (2011). Evolutionarily conserved surface residues constitute actin binding sites of tropomyosin. Proc Natl Acad Sci USA 108, 10150–10155.

Borovikov YS, Karpicheva OE, Chudakova GA, Robinson P, Redwood CS (2009). Dilated cardiomyopathy mutations in alpha-tropomyosin inhibit its movement during the ATPase cycle. Biochem Biophys Res Commun 381, 403–406.

Chalovich JM, Eisenberg E (1982). Inhibition of actomyosin ATPase activity by troponin-tropomyosin without blocking the binding of myosin to actin. J Biol Chem 257, 2432–2437.

Chereau D, Boczkowska M, Skwarek-Maruszewska A, Fujiwara I, Hayes DB, Rebowski G, Lappalainen P, Pollard TD, Dominguez R (2008). Leiomodin is an actin filament nucleator in muscle cells. Science 320, 239–243.

Colpan M, Ly T, Grover S, Tolkatchev D, Kostyukova AS (2017). The cardiomyopathy-associated K15N mutation in tropomyosin alters actin filament pointed end dynamics. Arch Biochem Biophys 630, 18–26.

Colpan M, Moroz NA, Gray KT, Cooper DA, Diaz CA, Kostyukova AS (2016a). Tropomyosin-binding properties modulate competition between tropomodulin isoforms. Arch Biochem Biophys 600, 23–32.

Colpan M, Tolkatchev D, Grover S, Helms GL, Cort JR, Moroz N, Kostyukova AS (2016b). Localization of the binding interface between leiomodin-2 and alpha-tropomyosin. Biochim Biophys Acta 1864, 523–530.

Conley CA, Fritz-Six KL, Almenar-Queralt A, Fowler VM (2001). Leiomodins: larger members of the tropomodulin (Tmod) gene family. Genomics 73, 127–139.

Cooper JA, Walker SB, Pollard TD (1983). Pyrene actin: documentation of the validity of a sensitive assay for actin polymerization. J Muscle Res Cell Motil 4, 253–262.

Dong WJ, Chandra M, Xing J, She M, Solaro RJ, Cheung HC (1997a). Phosphorylation-induced distance change in a cardiac muscle troponin I mutant. Biochemistry 36, 6754–6761.

Dong WJ, Chandra M, Xing J, Solaro RJ, Cheung HC (1997b). Conformation of the N-terminal segment of a monocysteine mutant of troponin I from cardiac muscle. Biochemistry 36, 6745–6753.
Dong WJ, Xing J, Robinson JM, Cheung HC (2001). Ca(2+) induces an extended conformation of the inhibitory region of troponin I in cardiac muscle troponin. J Mol Biol 314, 51–61.
Du CK, Morimoto S, Nishii K, Minakami R, Ohta M, Tadano N, Lu QW, Wang YY, Zhan DY, Mochizuki M, *et al*. (2007). Knock-in mouse model of dilated cardiomyopathy caused by troponin mutation. Circ Res 101, 185–194.
Edelhoch H (1967). Spectroscopic determination of tryptophan and tyrosine in proteins. Biochemistry 6, 1948–1954.
Fabiato A (1988). Computer programs for calculating total from specified free or free from specified total ionic concentrations in aqueous solutions containing multiple metals and ligands. Methods Enzymol 157, 378–417.
Fasman GD (1989). Practical Handbook of Biochemistry and Molecular Biology, Boca Raton, FL: CRC Press.
Fokstuen S, Munoz A, Melacini P, Iliceto S, Perrot A, Ozcelik C, Jeanrenaud X, Rieubland C, Farr M, Faber L, *et al*. (2011). Rapid detection of genetic variants in hypertrophic cardiomyopathy by custom DNA resequencing array in clinical practice. J Med Genet 48, 572–576.
Frey N, Luedde M, Katus HA (2011). Mechanisms of disease: hypertrophic cardiomyopathy. Nat Rev Cardiol 9, 91–100.
Fritz-Six KL, Cox PR, Fischer RS, Xu B, Gregorio CC, Zoghbi HY, Fowler VM (2003). Aberrant myofibril assembly in tropomodulin1 null mice leads to aborted heart development and embryonic lethality. J Cell Biol 163, 1033–1044.
Frye J, Klenchin VA, Rayment I (2010). Structure of the tropomyosin overlap complex from chicken smooth muscle: insight into the diversity of N-terminal recognition. Biochemistry 49, 4908–4920.
Geeves MA (2012). Thin filament regulation. In: Comprehensive Biophysics, ed. EH Egelman, Oxford, UK: Elsevier, 251–267.
Greenfield NJ, Huang YJ, Swapna GV, Bhattacharya A, Rapp B, Singh A, Montelione GT, Hitchcock-DeGregori SE (2006). Solution NMR structure of the junction between tropomyosin molecules: implications for actin binding and regulation. J Mol Biol 364, 80–96.
Gregorio CC, Fowler VM (1995). Mechanisms of thin filament assembly in embryonic chick cardiac myocytes: tropomodulin requires tropomyosin for assembly. J Cell Biol 129, 683–695.
Gunning PW, Hardeman EC, Lappalainen P, Mulvihill DP (2015). Tropomyosin—master regulator of actin filament function in the cytoskeleton. J Cell Sci 128, 2965–2974.
Guo X, Wattanapermpool J, Palmiter KA, Murphy AM, Solaro RJ (1994). Mutagenesis of cardiac troponin I. Role of the unique NH2-terminal peptide in myofilament activation. J Biol Chem 269, 15210–15216.
Guth K, Potter JD (1987). Effect of rigor and cycling cross-bridges on the structure of troponin C and on the Ca2+ affinity of the Ca2+-specific regulatory sites in skinned rabbit psoas fibers. J Biol Chem 262, 13627–13635.
Helfman DM, Berthier C, Grossman J, Leu M, Ehler E, Perriard E, Perriard JC (1999). Nonmuscle tropomyosin-4 requires coexpression with other low molecular weight isoforms for binding to thin filaments in cardiomyocytes. J Cell Sci 112 (Pt 3), 371–380.
Hernandez OM, Housmans PR, Potter JD (2001). Invited Review: pathophysiology of cardiac muscle contraction and relaxation as a result of alterations in thin filament regulation. J Appl Physiol 90, 1125–1136.
Hershberger RE, Morales A (1993). Dilated cardiomyopathy overview. In: GeneReviews((R)), ed. MP Adam, HH Ardinger, RA Pagon, SE Wallace, LJH Bean, K Stephens, and A Amemiya, Seattle: University of Washington.
Hershberger RE, Norton N, Morales A, Li D, Siegfried JD, Gonzalez-Quintana J (2010). Coding sequence rare variants identified in MYBPC3, MYH6, TPM1, TNNC1, and TNNI3 from 312 patients with familial or idiopathic dilated cardiomyopathy. Circ Cardiovasc Genet 3, 155–161.
Hershberger RE, Pinto JR, Parks SB, Kushner JD, Li D, Ludwigsen S, Cowan J, Morales A, Parvatiyar MS, Potter JD (2009). Clinical and functional characterization of TNNT2 mutations identified in patients with dilated cardiomyopathy. Circ Cardiovasc Genet 2, 306–313.
Jin JP, Chong SM (2010). Localization of the two tropomyosin-binding sites of troponin T. Arch Biochem Biophys 500, 144–150.
Kostyukova A, Maeda K, Yamauchi E, Krieger I, Maeda Y (2000). Domain structure of tropomodulin: distinct properties of the N-terminal and C-terminal halves. Eur J Biochem 267, 6470–6475.
Kostyukova AS, Hitchcock-DeGregori SE (2004). Effect of the structure of the N terminus of tropomyosin on tropomodulin function. J Biol Chem 279, 5066–5071.
Kouyama T, Mihashi K (1981). Fluorimetry study of N-(1-pyrenyl)iodoacetamide-labelled F-actin. Local structural change of actin protomer both on polymerization and on binding of heavy meromyosin. Eur J Biochem 114, 33–38.
Leinweber B, Tang JX, Stafford WF, Chalovich JM (1999). Calponin interaction with alpha-actinin-actin: evidence for a structural role for calponin. Biophys J 77, 3208–3217.
Li XE, Tobacman LS, Mun JY, Craig R, Fischer S, Lehman W (2011). Tropomyosin position on F-actin revealed by EM reconstruction and computational chemistry. Biophys J 100, 1005–1013.
Liu H, Naismith JH (2008). An efficient one-step site-directed deletion, insertion, single and multiple-site plasmid mutagenesis protocol. BMC Biotechnol 8, 91.
Ly T, Krieger I, Tolkatchev D, Krone C, Moural T, Samatey FA, Kang C, Kostyukova AS (2018). Structural destabilization of tropomyosin induced by the cardiomyopathy-linked mutation R21H. Protein Sci 27, 498–508.
Ly T, Moroz N, Pappas CT, Novak SM, Tolkatchev D, Wooldridge D, Mayfield RM, Helms G, Gregorio CC, Kostyukova AS (2016). The N-terminal tropomyosin- and actin-binding sites are important for leiomodin 2's function. Mol Biol Cell 27, 2565–2575.
Lymn RW, Taylor EW (1970). Transient state phosphate production in the hydrolysis of nucleoside triphosphates by myosin. Biochemistry 9, 2975–2983.
Lymn RW, Taylor EW (1971). Mechanism of adenosine triphosphate hydrolysis by actomyosin. Biochemistry 10, 4617–4624.
Maron BJ (2002). Hypertrophic cardiomyopathy: a systematic review. J Am Med Assoc 287, 1308–1320.
Maron BJ, Doerer JJ, Haas TS, Tierney DM, Mueller FO (2009). Sudden deaths in young competitive athletes: analysis of 1866 deaths in the United States, 1980–2006. Circulation 119, 1085–1092.
Maron BJ, Towbin JA, Thiene G, Antzelevitch C, Corrado D, Arnett D, Moss AJ, Seidman CE, Young JB, American Heart Association, *et al*. (2006). Contemporary definitions and classification of the cardiomyopathies: an American Heart Association Scientific Statement from the Council on Clinical Cardiology, Heart Failure and Transplantation Committee; Quality of Care and Outcomes Research and Functional Genomics and Translational Biology Interdisciplinary Working Groups; and Council on Epidemiology and Prevention. Circulation 113, 1807–1816.
Mathur MC, Chase PB, Chalovich JM (2011). Several cardiomyopathy causing mutations on tropomyosin either destabilize the active state of actomyosin or alter the binding properties of tropomyosin. Biochem Biophys Res Commun 406, 74–78.
McGhee JD, von Hippel PH (1974). Theoretical aspects of DNA-protein interactions: co-operative and non-co-operative binding of large ligands to a one-dimensional homogeneous lattice. J Mol Biol 86, 469–489.
McKillop DF, Geeves MA (1993). Regulation of the interaction between actin and myosin subfragment 1: evidence for three states of the thin filament. Biophys J 65, 693–701.
McLachlan AD, Stewart M (1976). The 14-fold periodicity in alpha-tropomyosin and the interaction with actin. J Mol Biol 103, 271–298.
Mirza M, Marston S, Willott R, Ashley C, Mogensen J, McKenna W, Robinson P, Redwood C, Watkins H (2005). Dilated cardiomyopathy mutations in three thin filament regulatory proteins result in a common functional phenotype. J Biol Chem 280, 28498–28506.
Mirza M, Robinson P, Kremneva E, Copeland O, Nikolaeva O, Watkins H, Levitsky D, Redwood C, El-Mezgueldi M, Marston S (2007). The effect of mutations in alpha-tropomyosin (E40K and E54K) that cause familial dilated cardiomyopathy on the regulatory mechanism of cardiac muscle thin filaments. J Biol Chem 282, 13487–13497.
Monteiro PB, Lataro RC, Ferro JA, Reinach Fde C (1994). Functional alpha-tropomyosin produced in Escherichia coli. A dipeptide extension can substitute the amino-terminal acetyl group. J Biol Chem 269, 10461–10466.
Murakami K, Stewart M, Nozawa K, Tomii K, Kudou N, Igarashi N, Shirakihara Y, Wakatsuki S, Yasunaga T, Wakabayashi T (2008). Structural basis for tropomyosin overlap in thin (actin) filaments and the generation of a molecular swivel by troponin-T. Proc Natl Acad Sci USA 105, 7200–7205.
Ohtsuki I (1979). Molecular arrangement of troponin-T in the thin filament. J Biochem 86, 491–497.
Ouyang Y, Mamidi R, Jayasundar JJ, Chandra M, Dong WJ (2010). Structural and kinetic effects of PAK3 phosphorylation mimic of cTnI(S151E) on the cTnC-cTnI interaction in the cardiac thin filament. J Mol Biol 400, 1036–1045.
Palm T, Graboski S, Hitchcock-DeGregori SE, Greenfield NJ (2001). Disease-causing mutations in cardiac troponin T: identification of a critical tropomyosin-binding region. Biophys J 81, 2827–2837.

Pappas CT, Mayfield RM, Henderson C, Jamilpour N, Cover C, Hernandez Z, Hutchinson KR, Chu M, Nam KH, Valdez JM, *et al*. (2015). Knockout of Lmod2 results in shorter thin filaments followed by dilated cardiomyopathy and juvenile lethality. Proc Natl Acad Sci USA 112, 13573–13578.
Parry DA, Squire JM (1973). Structural role of tropomyosin in muscle regulation: analysis of the x-ray diffraction patterns from relaxed and contracting muscles. J Mol Biol 75, 33–55.
Paul DM, Morris EP, Kensler RW, Squire JM (2009). Structure and orientation of troponin in the thin filament. J Biol Chem 284, 15007–15015.
Paul DM, Squire JM, Morris EP (2017). Relaxed and active thin filament structures; a new structural basis for the regulatory mechanism. J Struct Biol 197, 365–371.
Pearlstone JR, Smillie LB (1977). The binding site of skeletal alpha-tropomyosin on troponin-T. Can J Biochem 55, 1032–1038.
Pirani A, Vinogradova MV, Curmi PM, King WA, Fletterick RJ, Craig R, Tobacman LS, Xu C, Hatch V, Lehman W (2006). An atomic model of the thin filament in the relaxed and Ca2+-activated states. J Mol Biol 357, 707–717.
Pirani A, Xu C, Hatch V, Craig R, Tobacman LS, Lehman W (2005). Single particle analysis of relaxed and activated muscle thin filaments. J Mol Biol 346, 761–772.
Poole KJ, Lorenz M, Evans G, Rosenbaum G, Pirani A, Craig R, Tobacman LS, Lehman W, Holmes KC (2006). A comparison of muscle thin filament models obtained from electron microscopy reconstructions and low-angle X-ray fibre diagrams from non-overlap muscle. J Struct Biol 155, 273–284.
Redwood C, Robinson P (2013). Alpha-tropomyosin mutations in inherited cardiomyopathies. J Muscle Res Cell Motil 34, 285–294.
Rieck DC, Dong W-J (2014). Conformational states and behavior of the heterotrimeric troponin complex. In: Troponin: Regulator of Muscle Contraction, ed. J-P Jin, New York: Nova Science Publishers, 91–196.
Risi C, Eisner J, Belknap B, Heeley DH, White HD, Schroder GF, Galkin VE (2017). Ca(2+)-induced movement of tropomyosin on native cardiac thin filaments revealed by cryoelectron microscopy. Proc Natl Acad Sci USA 114, 6782–6787.
Robinson JM, Dong WJ, Xing J, Cheung HC (2004). Switching of troponin I: Ca(2+) and myosin-induced activation of heart muscle. J Mol Biol 340, 295–305.
Robinson P, Mirza M, Knott A, Abdulrazzak H, Willott R, Marston S, Watkins H, Redwood C (2002). Alterations in thin filament regulation induced by a human cardiac troponin T mutant that causes dilated cardiomyopathy are distinct from those induced by troponin T mutants that cause hypertrophic cardiomyopathy. J Biol Chem 277, 40710–40716.
Rusconi P, Wilkinson JD, Sleeper LA, Lu M, Cox GF, Towbin JA, Colan SD, Webber SA, Canter CE, Ware SM, *et al*. (2017). Differences in presentation and outcomes between children with familial dilated cardiomyopathy and children with idiopathic dilated cardiomyopathy: a report from the Pediatric Cardiomyopathy Registry Study Group. Circ Heart Fail 10.
Schlecht W, Zhou Z, Li KL, Rieck D, Ouyang Y, Dong WJ (2014). FRET study of the structural and kinetic effects of PKC phosphomimetic cardiac troponin T mutants on thin filament regulation. Arch Biochem Biophys 550–551, 1–11.
She M, Dong WJ, Umeda PK, Cheung HC (1998). Tryptophan mutants of troponin C from skeletal muscle–an optical probe of the regulatory domain. Eur J Biochem 252, 600–607.
Singh A, Hitchcock-DeGregori SE (2007). Tropomyosin's periods are quasi-equivalent for actin binding but have specific regulatory functions. Biochemistry 46, 14917–14927.
Skwarek-Maruszewska A, Boczkowska M, Zajac AL, Kremneva E, Svitkina T, Dominguez R, Lappalainen P (2010). Different localizations and cellular behaviors of leiomodin and tropomodulin in mature cardiomyocyte sarcomeres. Mol Biol Cell 21, 3352–3361.
Sweeney HL, Houdusse A (2010). Structural and functional insights into the Myosin motor mechanism. Annu Rev Biophys 39, 539–557.
Sweet M, Taylor MR, Mestroni L (2015). Diagnosis, prevalence, and screening of familial dilated cardiomyopathy. Expert Opin Orphan Drugs 3, 869–876.
Szatmari D, Bugyi B, Ujfalusi Z, Grama L, Dudas R, Nyitrai M (2017). Cardiac leiomodin2 binds to the sides of actin filaments and regulates the ATPase activity of myosin. PLoS One 12, e0186288.
Takeda S, Yamashita A, Maeda K, Maeda Y (2003). Structure of the core domain of human cardiac troponin in the Ca(2+)-saturated form. Nature 424, 35–41.
Tsukada T, Pappas CT, Moroz N, Antin PB, Kostyukova AS, Gregorio CC (2010). Leiomodin-2 is an antagonist of tropomodulin-1 at the pointed end of the thin filaments in cardiac muscle. J Cell Sci 123, 3136–3145.
Vinogradova MV, Stone DB, Malanina GG, Karatzaferi C, Cooke R, Mendelson RA, Fletterick RJ (2005). Ca(2+)-regulated structural changes in troponin. Proc Natl Acad Sci USA 102, 5038–5043.
Wang Y, Xu Y, Guth K, Kerrick WG (1999). Troponin C regulates the rate constant for the dissociation of force-generating myosin cross-bridges in cardiac muscle. J Muscle Res Cell Motil 20, 645–653.
Weber A, Pennise CR, Babcock GG, Fowler VM (1994). Tropomodulin caps the pointed ends of actin filaments. J Cell Biol 127, 1627–1635.
Weber A, Pennise CR, Fowler VM (1999). Tropomodulin increases the critical concentration of barbed end-capped actin filaments by converting ADP.P(i)-actin to ADP-actin at all pointed filament ends. J Biol Chem 274, 34637–34645.
Wulf SF, Ropars V, Fujita-Becker S, Oster M, Hofhaus G, Trabuco LG, Pylypenko O, Sweeney HL, Houdusse AM, Schroder RR (2016). Force-producing ADP state of myosin bound to actin. Proc Natl Acad Sci USA 113, E1844–E1852.
Xing J, Cheung HC (1994). Vanadate-induced changes in myosin subfragment-1 from cardiac muscle. Arch Biochem Biophys 313, 229–234.
Xing J, Jayasundar JJ, Ouyang Y, Dong WJ (2009). Forster resonance energy transfer structural kinetic studies of cardiac thin filament deactivation. J Biol Chem 284, 16432–16441.
Yang S, Barbu-Tudoran L, Orzechowski M, Craig R, Trinick J, White H, Lehman W (2014). Three-dimensional organization of troponin on cardiac muscle thin filaments in the relaxed state. Biophys J 106, 855–864.
Zhou Z, Li KL, Rieck D, Ouyang Y, Chandra M, Dong WJ (2012). Structural dynamics of C-domain of cardiac troponin I protein in reconstituted thin filament. J Biol Chem 287, 7661–7674.